Founded 1905

MODELING AND CONTROL OF HARD DISK DRIVE IN MOBILE APPLICATIONS

PHYO PHYO SAN

(***B.Eng.*** & ***M.Sc.***)

A THESIS SUBMITTED

FOR THE DEGREE OF MASTER OF ENGINEERING

DEPARTMENT OF ELECTRICAL & COMPUTER ENGINEERING

NATIONAL UNIVERSITY OF SINGAPORE

2009

Acknowledgements

First of all, I would like to express my heartfelt appreciation to my supervisor, Professor Shuzhi Sam Ge, for his remarkable guidance to successfully complete this thesis and giving me a chance to work on this research project.

I also would like express my sincere gratitude to my co-supervisor, Professor Tong Heng Lee for his suggestions and remarks on many occasions that are extremely helpful in improving my research work.

I am very grateful to Dr. Venkatakrishnan Venkataramanan who gave me guidance into the field of disk drive servo technology and the efficient methodologies of research.

I would like to thanks to all my colleagues and friends in the Mechatronics and Automation Lab and the Edutainment Robotics Lab for their concerns and help.

Special thanks to all the staff and students in the division of Mechatronics and Recording Channel in Data Storage Institute (DSI). Due to their great help, I have a chance to learn the basics of disk drive servo systems and to set up the experimental platform.

Latest but not least, I wish to express my deepest appreciation to my family for their understanding, encouragement and support throughout my studies.

Contents

Summary

The most important changes in hard disk drive (HDD) technology has been the rapid increase in data storage density due to the rising demand in data storage systems. High performance servo controllers are needed as data are accessed via the electro-mechanical voice-coil motor (VCM) actuator. Most of the servo systems use a VCM actuator to actuate the read/write (R/W) recording arm assembly which consists of a pivot with a ball bearing, a metal arm, and a rigid suspension that holds the R/W head and slider.

To come up with devices that are smaller, cheaper and able to store more data and retrieve them with faster speed, the presence of friction in the rotary actuator pivot bearing becomes a more noticeable issues in the HDD industries. The pivot friction hysteresis nonlinearity introduced by the bearing of the actuator pivot results in large residual errors and high-frequency oscillations, which may produce larger positioning error signal to hold back the further decreasing of the track width and to deteriorate the performance of servo systems. Thus, it is highly desirable to characterize the

behaviors of friction nonlinearities in the HDD servo systems. This thesis presents a fairly comprehensive modeling and compensation of pivot friction hysteresis nonlinearity of a typical VCM actuator used in commercial HDDs and a practical account of the application of an improved adaptive neural network (NN) controller to VCM of HDDs.

In this thesis, a brief introduction of HDD servo technology and the prevalent trend in hard disk design towards smaller hard disks with increasingly larger capacities are presented. Followed by a brief overview of HDD head positioning servomechanism, the fundamental components of an HDD servo system are introduced. A comprehensive studies of the commonly used classical friction models including both static and dynamic models are presented for comparison and controller design. Besides, a complete model of the VCM actuator including pivot friction hysteresis nonlinearity is obtained through a careful examination of the configuration and structure of actual system and through a thorough analysis of its physical effects in frequency domain response.

In addition, a systematic treatment of adaptive neural network (NN) friction compensation techniques is presented from theoretical aspects in order to achieve high precision motion control. By considering the position and velocity tracking control of hard disk drive servo mechanism with friction, an improved adaptive NN friction compensation is given based on the dynamic LuGre friction model. To achieve asymptotic tracking of the desired trajectory and guarantee the boundedness of all signals

in the closed loop, an adaptive neural network (NN) control algorithm is designed by the use of Lyapunov synthesis.

Finally, experimental studies is conducted with commercially available 3.5-inch hard disk drive (Seagate Barracuda 7200.10), wherein the control objective is to track a reference trajectory with the presence of hysteresis friction nonlinearity from the pivot bearing. Extensive experimental results have shown that the proposed approaches are effective for friction compensation in hard disk drive servo mechanism. Thus, the conclusion is drawn by stating that the proposed adaptive NN control technique has a feature of removing the uncompensated portion of friction nonlinearity without sacrificing the overall tracking performance.

List of Figures

Notation

ADC	Analog-to-Digital Converter
DAC	Digital-to-Analog Converter
DSP	Digital Signal Processor
HDD	Hard Disk Drive
LDV	Laser Doppler Vibrometer
MEMS	Micro Electro-Mechanical System
NN	Neural Network
PD	Proportional Derivative
PES	Position Error Signal
PI	Proportional Integral
PID	Proportional Integral Derivative
TMR	Track Mis-Registration
TPI	Track Per Inch
VCM	Voice Coil Motor

Chapter 1

Introduction

The prevalent trend in hard disk design is towards smaller hard disks with increasingly larger capacities. This implies that the track width to be smaller, which leads to lower error tolerance in the positioning of the head. To meet with increasingly demand in hard disk drives, the most important change in hard disk drive technology has been carried out with an increase in data storage density. The HDD applications are expected to be seen in digital camera, car navigation and audio systems, and even mobile phones in the near future due to the ever increasing effort of HDDs areal density. The servo system must achieve precise positioning of read-write head (R/W) on a desired track (track following) and fast transition from one track to another targeted track (track seeking) within shortest track seeking time for faster data transmission rates.

In this chapter, some prevalent trends in the HDDs industry are examined in Section

1.1. The basic knowledge about the HDD and HDD servo system are introduced in Section 1.2. By discussing the recent research works in the track following control design for HDDs, the servo system and servo control challenges faced by servo engineers and researchers are presented in Section 1.3. The rigorous analysis on the various sources of disturbances, nonlinearities and uncertainties of a typical hard disk drive servo system are discussed in Section 1.3.1, 1.3.2 and 1.3.3 respectively. In Section 1.4, the objectives, scopes and organization of thesis is presented.

1.1 Disk Drive Technology Development Trend

The hard disk drive (HDD) is the most preferred data storage device due to its low cost, excellent scalability and the fact that it has highest areal density, largest capacity, highest transfer rate and highest access speed among data storage devices. With the rapid progresses of magnetic recording technologies, the data storage areal density of HDDs have been increasing dramatically through 1990's. Commercial disk drive areal density has reached approximately $120 Gb/in^2$ in 2005 and expected to achieve $100 Gb/in^2$ in 2009 under laboratory demonstration with possible commercialization in 2013 [5]. As can be seen in Figure 1.1, the earliest hard disk drives supported an real density of $2000 bits/in^2$. The increment in areal density has been achieved by a factor of 5 million as presented in Figure 1.1. Track density has been increased by reducing the off-track motion due to component disturbances and by improving the

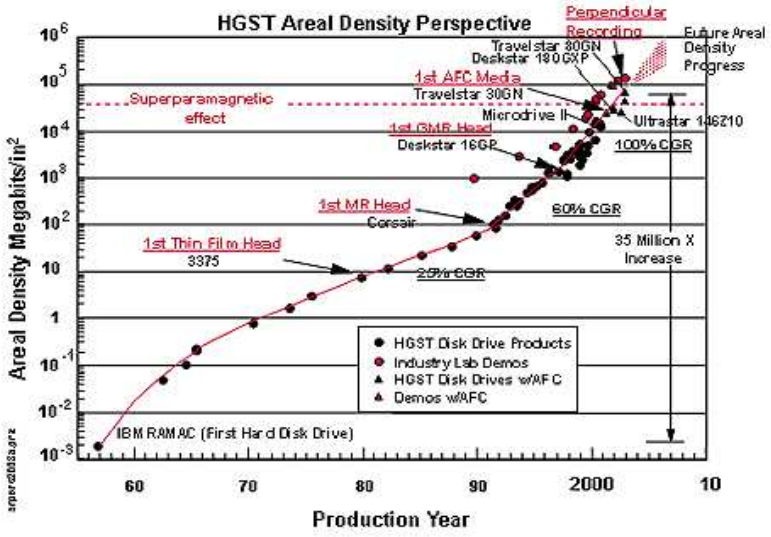

Figure 1.1: Trend in HDD areal density (source: [1])

ability of servo controller to regulate the head on narrower tracks.

The reduction on disk surface roughness, the quality of lubricant, the design of air bearing play in improving storage bit density. Since those factors allow the slider to fly in closer proximity of the disk, the bit size is reduced. In [6],[7], [8] and [9], it has been discussed that the flying height in today hard disk drives are about 5 nanometers (nm) while typical flying height in 1997 were 25 (nm). In addition, the data transfer rate has achieved more than $125 Mbits/s$ in today hard disk drives.

Since magnetic recording technology made continuous improvements in areal density, size and form factors of HDDs, the reduction in disk size and form factors are also significant in the evolutionary development of HDDs. Due to the diverse applications

of HDDs in consumer electronics devices, today's HDDs have form factors of 3.4", 2.5" and even 1" in micro hard disk drives.

As technology advances, the significant reduction in disk size and form factors, increase in areal density and faster data transfer rate are highly desirable. With more data being packed into a smaller space, servo positioning during data access operation with the presence of larger amount of windage disturbances and other nonlinearities become a challenge for HDD servo system.

1.2 Overview of Hard Disk Drive System

The HDD is a mechatronic system and it includes several components that can be broadly classified into magnetic components, mechanical components, electromechanical components and electronics. In [1], it has been explained that the media and the head are magnetic components of hard disk drive system and those are assigned to be used in storage and retrieval of binary information. In HDD, the information is recorded and retrieved using the read/write head since the information bits are stored in concentric data tracks on a rotating disk that is coated with magnetic media. Practical realization of such non-volatile storage and retrieval of binary bits involves many other essential components such as a motor to spin the disks, an actuator to make R/W head access the desired data etc. As presented in [2], the essential components found in typical HDD can be clearly seen in Figure 1.2. The

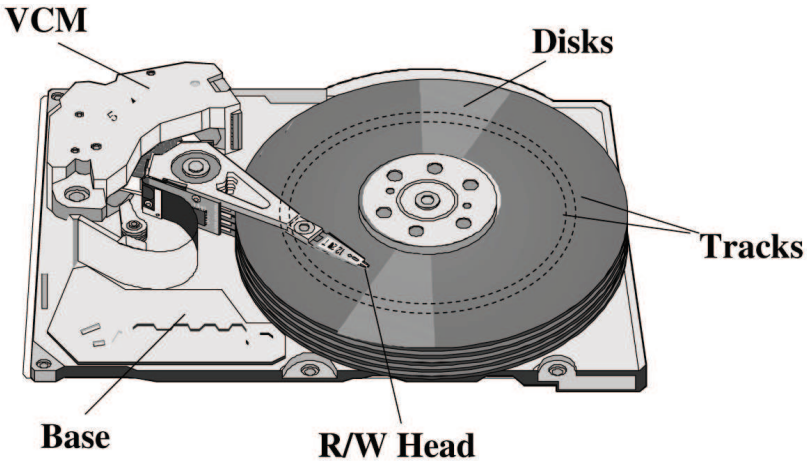

Figure 1.2: Overview of hard disk drive system

main functions and special features of those components are briefly explained in this section.

Disk: A typical hard disk drive includes one or more flat rotating disks with two magnetic surfaces that is called platters. The disk is mounted through a hole at the center on the spindle of a motor for spinning of the disks. The data are recorded on a continuously spinning disks which are made of aluminum or glass and coated with a thin layer of magnetic material on both sides of a disk. To produce uniform readback signal from the R/W heads that is flying a few nanometers above the disk surface, the surface of the disk must be smooth. To ensure a very smooth surface, the surface of each disk are precision machined and paid carefully attention to remove any imperfections during the manufacturing process. However, the smooth disk drives gives rise to a problem of producing stiction force when the R/W head touches the disk surface if there is no disk rotation and no air bearing is formed. To solve the

problem of stiction between head and disk, several methods have been proposed in [10].

Head/Suspension Assembly: In HDDs, the R/W head are of ferrite, metal-in-gap, thin-film or magnetoresistive (MR) types in which ferrite, metal-in-gap and thin film types are used the principle of electromagnetic induction effect and that are generally found in older types of R/W heads. In modern HDDs, the R/W head is a thin-flim, metalized structure that exhibits magneto-resistive effect, in which the resistivity changes when it is brought under the influence of a magnetic field. The voltage across the MR sensor is obtained when a current flow through the MR head. The voltage is a direct measurement of the magnetic field produced by binary bits written on the disk surface. Both read and write operations in older disk drives were performed by single head, while the modern HDDs use separated head for read and write operations. These heads are referred to as a slider when those are positioned only microinches above the recording medium on an air-bearing surface. A gimbal attaches the slider to a suspension for pitch and roll rotations, while the suspension is attached to the arm of the actuator by a ball swaging.

Actuator Assembly: In a hard disk drive system, a set of actuator assembly is employed to position the read/write head on the certain track on the disk surface. This actuator assembly consists of a VCM, data flex cable or printed circuit cable, actuator arms and crash-stops at both ends of travel. The data are read/written from/to the magnetic disk surfaces by the use of R/W heads mounted on the slider

which is attached to the actuator arm. The function of actuator in HDD that is so called VCM actuator is the same as a loud speaker. The coil of the VCM actuator extends between a yoke/magnets. The VCM driver or amplifier are also part of the actuator assembly which is mainly used to drive or give the power to the VCM actuator.

Spindle and Motor Assembly: Brushless DC motor is responsible to spin the stack of disks in HDD with stable, reliable and consistent turning power for thousands of hours. All hard disks use servo-controlled DC spindle motor and are configured for direct connection without the use of no belts or gears when it is connected to the hard disk platter. The fluid dynamic bearing or aerodynamic bearing spindles are normally used in high performance hard disk drives in which the spindle speed is around 10,000 RPM or more. Many models of hard disk drives for the desktop and mobile environment are still using the spindle speed of 5,400 RPM or 6,000 RPM while high performance hard disk drives are using higher spinning rates such as 7,200 RPM, 10,000 RPM or even 15,000 RPM. The most critical component in hard disk's spindle motor is the set of spindle motor bearings at each end of the spindle shaft. With the demand for higher areal density and faster spindle speed, the fluid dynamic bearing (FDB) spindle motor are adopted in HDDs. In ball bearing motors, it is impossible to make the ball and race of the bearings perfect and free from the defects due to the existence of mechanical contact between the ball and race of the bearing. In addition, the variation in spindle speed is a major source of disturbance in the

tracking servo loop and the speed of the motors must be precisely controlled.

Electronic Card: The electronic card behave as an interface to the host personal computer. The widely used integrated electronic circuit in hard disk drives are the Integrated Drive Electronics (IDE), the Advanced Technology Attachment (ATA), and the Small Computer System Interface (SCSI). These integrated circuits have a power driver for the spindle motor, VCM, R/W electronics, servo demodulator, microcontroller or digital signal processor (DSP) for servo control, ROM and RAM for microcode and data transfer.

Device Encloser: This is the most important component in hard disk drives because it determines the reliability of the disk drives and helps to keep the contamination low. It also keeps out dust and other contamination that are harmful to the R/W heads and the platters with the aid of recirculation and a breather filter. By doing so, the possibility of head crashes are also reduced. A gasket is used a seal between the top cover and the base casting that provides supports for the spindle, actuator, VCM yoke and electronics card.

1.3 HDD Servo System and Servo Control Challenges

A servomechanism or servo is a control system which has the specific task in controlling the position and velocity of a mechanical plant in which the actuator is responsible for the actual motion. In direct access storage devices, the servomechanism is called

the head-positioning servomechanism (HPS) as shown in Figure 1.3. In a hard disk drive system, head positioning servomechanism is a system to control the R/W heads of a disk drive to move from one track to another track or to follow the desired track [11].

The two major functions of head positioning servo mechanisms are track seeking and track following, which have two basic problems of servo control. The head positioning servomechanism moves the R/W head as fast as possible from one track to another when asked by the host system (Track Seeking). Once the head reaches the target track, it is regulated precisely over the track so that the PES is minimized (Track Following). Another important feature expected in HDD servomechanism is the smooth settling while the transition occur between the track seeking and track following modes without any jerk. The detailed description of servo modes in an HDD has been clearly explained in [2] as shown in Figure 1.4.

The nature of track seeking control is to force the actuator angular velocity to follow an ideal angular velocity profile that will guarantee the shortest possible seek time with minimum jerk. The data access time during read/wite head operation will be reduced due to fast seeking. The smooth seeking would yield less acoustic noise to have better performance of HDD in consumer electronic appliances. When the actuator is less than one track pitch away from the target track, the settling mode takes over from the seeking to following mode. In the HDD servo design, two different types of controllers are used for track-seeking and track-following. The mode switching

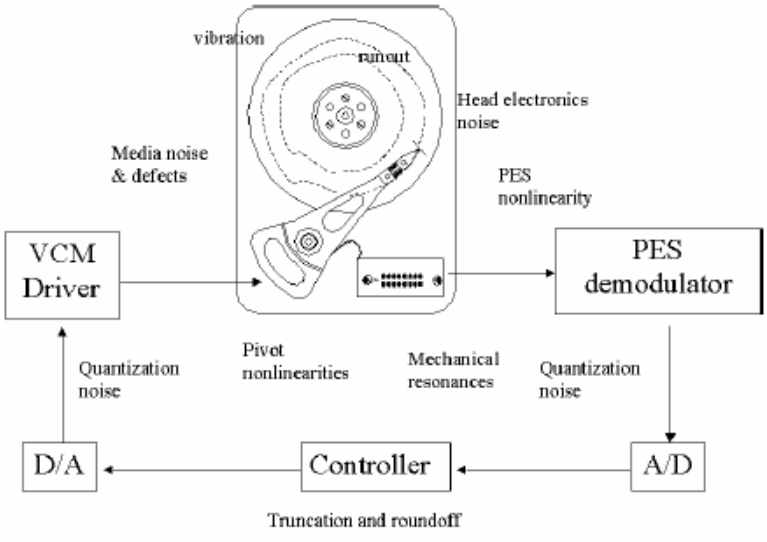

Figure 1.3: Typical servo loop in HDDs (source: [2])

control is usually adopted in the transient process so that the center of the recording head is kept within a certain position error tolerance of the target track center line for a fast control mode switching. Usually a control system is designed under the assumption that the initial vales are zero. However, in this case, the initial states of the track-following mode cannot be ignored since the "initial" means a time at mode switching and state variables such as velocity and position may have non-zero values. Those initial states may cause undesirable settling response if not being compensated. In [12], a nonlinear feedback control with time-varying damping factor was proposed for better settling response.

In the track following mode, the servo objective is to stay as close to the track center line as possible while reading and writing information. The control objective of HDD

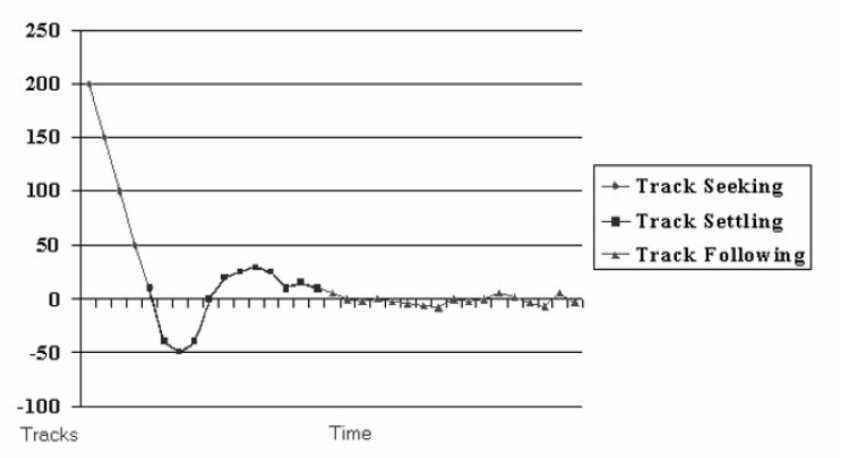

Figure 1.4: Track seeking and following of an HDD servo system (source:[2])

track-following control is to track a desired trajectory, where the desired output can be treated as a known signal and the actual output can be measured to use as a feedback signal in control algorithm. On the other hand, the HDD track-following controller must be able to compensate in Position Error Signal (PES), which is the difference between the desired track position and the actual head position. In the track-following control, the actuator saturation is not explicitly considered and the feedback controller is designed primarily based on linear control theory for stability such as PID (Proportional Integral Derivative) and lead-leg compensator. These feedback controllers are not enough for accurate positioning due to the presence of various disturbance sources, noise and other nonlinearities exist in the servo channel.

In [13], it has been presented that the performance of positioning is evaluated by

TMR which is defined by the standard deviation of PES ($\pm 3\sigma$):

$$TMR = 3\sigma = \sqrt[3]{\int_0^\infty P(\omega)\, d\omega} \tag{1.1}$$

where ω is radian frequency; $P(\omega)$ is the power spectral density of PES. The TMR in track-following is about 10% of the track width.

In smaller drive with larger capacity, the absolute track-following error with respect to target track center, which is commonly called TMR must be less than 10% of track pitch. As an instant, the track pitch is about $1\mu m$ and its TMR must be less than $0.1\mu m$ for 3.5 inches HDD with 25 kTPI, as stated in [2]. The goal of servo system is to minimize the TMR in the presence of measurement and process noise, disturbances and other nonlinearities which have been neglected in earlier control designs. As the TPI increases and the track pitch decreases, the increased level various PES error sources becomes more challenges due to decrease in the allowable variation of TMR. In [14] of Figure 1.3, the sources of TMR are due to the following errors listed roughly as follows:

- External shock and vibration present in portable devices;
- TMR caused by bearing hysteresis and poor velocity estimates during track settling mode;
- Servo pattern nonlinearities and inaccuracies caused by head, media and servo writing effects;

- Mechanical resonances in suspension, actuator, disk and housing;
- Electronic noise in recording channel entering the servo demodulator;
- Non-repeatable spindle runout caused by bearings;
- Repeatable Run Out (RRO) caused by thermal and other drifts and spindle.

To meet the increasing demand for higher TPI, the various errors sources and disturbances of servo channels and its compensation methods are analyzed in the following subsections 1.3.1 - 1.3.3.

1.3.1 Disturbance Rejection in HDD Servo System

As long as the applications of hard disk drives has extended to portable consumer electronic devices, the sources of disturbances such as input/output disturbances be come a major issue in HDDs head positioning servo mechanism. As the data density on magnetic disk drives has increased significantly, the data track width and the allowable position error has decreased. In mobile environment, the HDDs that suffer from external vibrations and shocks can degrade the tracking performance of read/write head and increase position error signal (PES). In Section 1.3, it has been discussed that higher TPI requires a tighter TMR which has a three times of the variance of the position error signals (PES), $3\Sigma_{pes}$. In variance of position error signals

Σ_{pes} can be approximated in 1.2 which discussed detailed in [2]

$$\sigma_{pes} = \sqrt{\frac{1}{N-1}\sum_{i=1}^{N} y_{pes}^2(i)} \tag{1.2}$$

where N is the number of sample.

There are several solutions that minimized the tracking performance of the R/W head subject to external vibrations and shocks of HDDs in mobile environment. To reduce the effect of the disturbances on HDDs, much of research work have been carried out in [15], [16] by the use of accelerometer to measure external disturbances and injecting the accelerometer signal to a feedforward controller. Several practical issues such as accelerometer beam resonances and varying accelerometer gains are discussed in [15] and those will hinder the full potential of acceleration feedforward schemes if not properly dealt with. To compensate for external vibration impact on the positioning accurcy of the VCM actuator, H-infinity control algorithm in state space has been successfully applied in [17]. In [18], the identification on both the plant and the disturbance model are considered and designed an adaptive feedforward controller as an add-on compensator to the existing compensator. For compensation of disturbance effects on the positioning accuracy, dual accelerometers are used in [19] to detect angular acceleration in HDDs. Adaptive feedforward control with the finite impulse response (FIR) filters was presented in [20]. However, the gradient algorithm for updating the coefficients of the FIR controller relies on the exact internal model. In [21], infinite impulse response (IIR) and the FIR filter based on the filtered-x lease mean square algorithm are developed to compensate for the effects of the disturbances.

Since the disturbance dynamic is highly nonlinear, it is difficult to be modeled accurately. To overcome those difficulties, neural networks as non-linear controllers have received considerable attention in the control of non-linear systems, because they offer distinct advantages over the conventional controller in achieving the desired performance in [22],[23], [24], [25] and [26]. Neural network feedforward controllers are designed in [27] for compensation of non-linear disturbance torque in seeker stabilizing loop, while the adaptive neural network feedforward compensator are designed in [28] for cancelation of nonlinear disturbance effects in ideal speed car engine controller.

1.3.2 Resonance Compensation in HDD Servo System

The various sources which contribute to TMR include vibrations caused by mechanical resonance subject to flexible structure of HDD actuator. Since the structure of HDD and actuator are not completely rigid, there exist hundreds of flexible modes which lead to vibrations and result in a longer settling time at the desired track. Each resonance mode can be modeled as a second-order transfer function and the VCM actuator transfer function displaying multiple resonance modes can be modeled as in [14]:

$$G(s) = \frac{k_t}{Js^2} \prod_{i=1}^{n} \frac{\omega_i^2}{s^2 + 2\varsigma_i \omega_i s + \omega_i^2} \tag{1.3}$$

where k_t is torque constant, J is inertia, and ς_i and ω_i are the damping ratio and the natural frequency of the i_{th} resonance mode. For simplicity, the frequency response

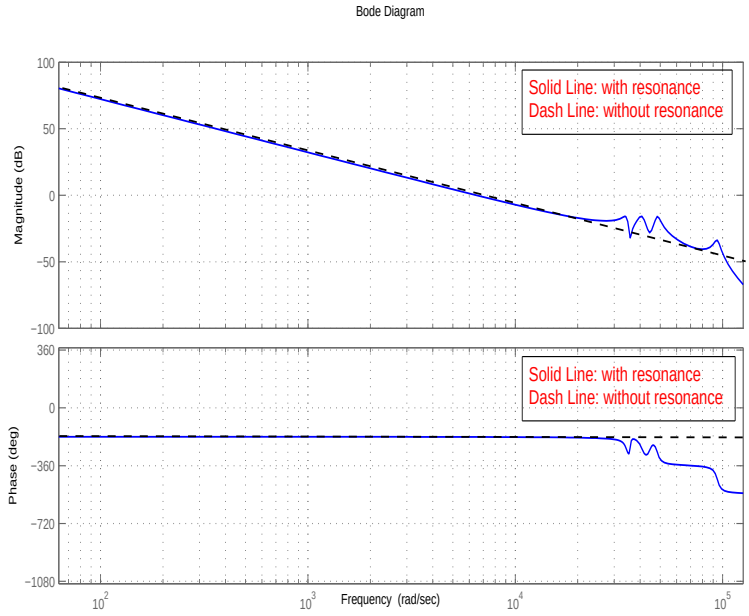

Figure 1.5: Frequency response of VCM actuator with resonance modes

characteristics with resonance modes in actuator dynamics for typical commercial hard disk drives are shown in Figure 1.5.

The mechanical resonances, if not being handled properly, will not only worsen the positioning accuracy, but will also lead the closed-loop system into instability. Typically, notch filters are used to suppress these mechanical resonance modes in [29], [30]. However, due to manufacturing tolerance, discrepancies in the resonance frequencies exist from drive to drive. In fact, it can also vary for single drive due to temperature changes, mechanical wear, excessive shock and disc distortion, all of which are common in HDD applications. Consequently, implementing filters with fixed notch frequencies do not consistently yield good performance.

The adaption algorithms for notch filters have been developed in [31]. The frequency characteristics of the open-loop transfer function, with and without notch filters are measured and the notch filters frequency adjusted iteratively until the frequency characteristics are congruent. Besides, indirect adaptive compensation (IAC) and structurally parallel compensation (SPC) were also proposed for resonant mode compensation in HDD dual stage actuation system in [32].

1.3.3 Friction Compensation in HDD Servo System

Owing to rapidly increasing demands for high capacity and performance of hard disk drives from industry, servo engineers are required to develop more advanced technologies. It is prospected that the position accuracy of hard disk drives will reach 25,000 TPI (less than 1 μ m per track) at the end of this century. For a system with such a high accuracy requirement, some nonlinearities currently being neglected or simplified in control system design must be taken into account and reconsidered. The nonlinearities preventing the system accuracy of a hard disk drive from further improvement include the ribbon flexibility, the windage and the nonlinear friction of the actuator pivot of a hard disk drive.

For a hard disk drive with positioning accuracy in the micrometer range or higher, friction dynamics in the pre-sliding stage cannot be neglected in control system design. Friction can cause many undesired effects such as steady state errors, tracking lag and limit cycles in servo system. For HDD control, one of the important tasks

during track following stage is to reduce the steady state error for improved positioning accuracy because friction reduces system gain in low frequency. In view of the difficulty in obtaining a true friction model, due to the nonlinearity and complexity of friction, no-model based robust friction compensation methods and its variations for implementation need to be investigated.

With portable applications becoming more significant, there has been a corresponding increase in demand for smaller hard disk drive with increasingly large data storage capacity. It is a challenge to design a controller that provides the necessary positioning accuracy to match the required track density with minimum tracking errors. Though several control methods have been successfully utilized to achieve this demand, the existence of nonlinearities and uncertainties in disk drive unit still remains obstacles for further enhancement in performance of positioning accuracy.

As can be seen in Figure 1.2, the R/W head is mounted on an VCM actuator assembly which is supported by a pivot cartridge consisting of a pair of preloaded ball bearings as shown in Figure 1.6. The R/W head positioning is controlled by a closed loop servo system where the actuator movement is driven by a vice coil motor. The friction in the actuator pivot bearing significantly deteriorates the performances of hard disk drive servo systems especially in small form factor hard disk drives. The residual errors caused by the friction make head positioning servo systems difficult to maintain the R/W head over the narrower track center. The mitigation of the friction is an ongoing issue since it becomes one of challenges to design hard disk drive servo systems for

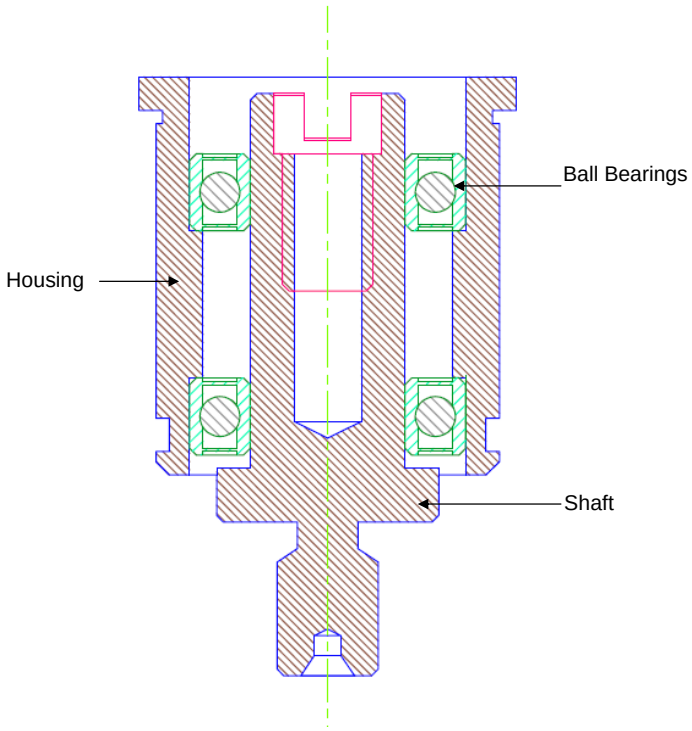

Figure 1.6: Pivot bearing in HDDs

small hard disk drives.

In order to capture the effects of pivot bearing friction in the servo control performance, various friction models have been investigated in [33]. The behavior of hysteresis friction torque of pivot bearing in HDD applications was investigated in [34]. Different models such as preload plus two-slope model and hysteretic two-slope model were studied in time domain [35] and frequency domain [36]. However, a signum function is used to describe Coulomb component of friction and this will result in a limit cycle characteristics in the velocity which should not happen in the presence of friction. In [37], a time-domain stick-slip friction was used to represent the pivot friction nonlinearity and a discrete-time disturbance observer was incorporated into

the conventional state feedback controller to compensate for the effect of pivot friction nonlinearity. However, as presented in [38], a stick slip model that is used to represent the friction nonlinearity is rather complicated and is not perfectly capture all characteristics of pivot friction nonlinearity. In [39], the pivot nonlinearity in HDD was modeled as a simplified Dahl model and a nonlinear compensator is designed based on the proposed model. Although the model proposed in [39] may match the measured data either in time domain or frequency domain, none of them can fit with the measured data very well. In [40], a servo system was designed using an enhanced composite nonlinear feedback (CNF) control technique with a simple friction and nonlinearity compensation scheme. To eliminate the effect of pivot friction nonlinearity, the compensator was designed by the use of an accelerometer and a disturbance observer in [41]. The disturbance observer was designed using Kalman filter framework and was implemented as an analog system to ensure a sufficiently wide bandwidth. However, the proposed control scheme required an accelerometer to be mounted on the arm for feedback signal. Although the cost and size of accelerometer have been significantly reduced by microelecromechanical (MEMS) technology, the reliability of an HDD system would have been distinctly reduced and cost also will be increased. In [42], a friction compensator was designed by using a newly proposed dynamic friction model structure. Besides, a disturbance observer was also designed based on the VCM current and the arm acceleration feedback signal. However, an effective Monte Carlo methods are still required to identify model parameters in the structure model. The

fuzzy logic model was obtained to approximate the pivot hysteresis nonlinearity in [43]. The obtained fuzzy actuator pivot model was augmented into a servo design to handle pivot nonlinearity by using it as a disturbance observer. Although the model results match the measured data very well, it may be too complicated in industrial applications.

Due to the capabilities of universal approximation, learning and adaption, parallel distributed structures of neural network, it has been specified as a suitable candidature for friction modeling and adaptive control design for friction compensation in [44] and [45]. By exploiting the benefit of good approximation property of NN, we develop an adaptive NN friction compensator, in this thesis, based on LuGre friction model for hard disk drive system subject to the pivot bearing hysteresis friction nonlinearity. The LuGre friction model introduced in [46] which capture all the static and dynamic characteristics of hysteresis friction nonlinearity. Compared with the compensation schemes in [41] [42] [43], in our method, no additional sensor/accelerometers are required to detect the effect of friction in hard disk drive system. Additionally, there is no specific methods for identification of friction model parameters due to good function approximation property of NN. Thus, the theoretically development of proposed adaptive friction compensator and its effectiveness can be seen experimentally in Chapter 4 and 5 respectively.

1.4 Objectives, Scope and Structure of Thesis

The main objective of this thesis is to develop adaptive friction compensator by the use of good approximation properties of neural network (NN) and investigate the improvements in settling time and positioning error signal as well. In this works, a most modest objective is to study the use of neural network as a strategy for the control of hard disk drive servo system with pivot friction hysteresis. The pivot nonlinearity of an HDD is investigated by adopting LuGre friction model model. In order to capture the time-varying uncertainties and nonlinearity, the adaptive tuning scheme is employed for the NN weights and the width of RBF functions. To compensate for the effect of the hysteresis friction nonlinearity, NN is adopted to approximate its unknown bounding function. With the proposed control, we try to ensure that all the closed-loop signals are bounded while the tracking error converges into a neighborhood of zero. In addition, we also carry out comprehensive comparisons studies between the conventional proportional-integral-derivative (PID) control (without friction compensator) and the proposed adaptive NN control (with friction compensator) in actual hard disk drive system. Additionally, an extensive experimental studies have been carried out to show that the proposed scheme has the advantages of fast convergence for both parameter estimation and tracking error to a neighborhood of zero.

To add more on the disadvantages of previous methods

In this thesis, an improved an improved adaptive NN friction compensator is designed

and developed for hard disk drive system subject to the pivot bearing hysteresis friction nonlinearity with the following contributions.

(i) the problem is reformulated as a mitigation of the unknown pivot bearing hysteresis friction nonlinearity problem in hard disk drive system;

(ii) the unknown approximation error bound resulting from neural networks is handled by adaptive bounding design; and

(iii) the effectiveness of the proposed method is practically investigated through extensive experimental results.

We can show that the proposed adaptive NN control not only reduces the effect of hysteresis friction nonlinearity, but also improves settling performance and tracking accuracy.

The thesis is organized as follows. Chapter 1 is an introductory chapter, representing the background studies of electro-mechanical systems, hard disk drive servo system. A brief account of the history of the hard disk drives and description of different components that make an HDD are provided. The trends in the HDD industry and the HDD servomechanism which is used to access data in a hard disk drives are also presented in this chapter. The detail studies of the control design issues that are related to the head positioning servomechanism are also provided in this section.

In Chapter 2. The preliminary studies of friction nonlinearity and commonly used

classical friction models for both static and dynamic characteristics are presented. Besides, the choice of nonlinear friction friction model through the use of frequency domain identification algorithm are also discussed. It is also verified that the chosen LuGre friction mdoel is quite well matched between observed response and actual response in frequency domain while the adopted LuGre friction model is quite well match with the actual friction model after carefully selecting different choices of parameter values.

Chapter 3 recalls some commonly used system identification and modeling techniques that are employed to identify the models of VCM actuators. The mathematical model of the VCM actuator and its model with current driver are also given in this chapter. In addition, an algorithm for identifying the transfer function model of hard disk drive system are also presented.

Chapter 4 of this thesis discusses for the design of an improved adaptive neural network (NN) control methodologies for friction compensation. For suppression of friction nonlinearity, an adaptive NN controller is designed by the use of LuGre dynamic friction model. To achieve asymptotic tracking of the desired trajectory and guarantee the boundedness of all signals in the closed loop, adaptive neural network (NN) control algorithm was designed using Lyapunov synthesis. To show the effectiveness of proposed friction compensator, the intensive simulation studies are carried also presented in this Chapter.

Chapter 5 begins with modeling and system identification of the VCM actuator including pivot friction hysteresis nonlinearity through a careful examination of actual system and thorough analysis of its physical effects in frequency domain. For controller assessment, experimental verification and its implementation results results are discussed, in this chapter, for tracking of sinusoidal and step demands. Extensive experimental results have shown that the proposed approach is effective for compensation of pivot hysteresis friction nonlinearity in hard disk drive servo system.

Chapter 6 summarizes the findings and results of this thesis and some possible future research are presented.

Chapter 2

Preliminaries studies

2.1 Introduction

As the microdrives become popular in these days with high demand from many new applications, many factors such as friction nonlinearities, disturbances and high frequency resonances are needed to be taken into consideration. Even though those factors can be safely neglected in normal drives, it becomes critical issues for micro hard disk drives. In this chapter, a comprehensive studies of nonlinear friction including static and dynamic of friction behaviors are discussed in Section 2.2. The choice of nonlinear friction friction model through the use of frequency domain identification algorithm is given Section in 2.3 before the conclusion of this chapter is presented in Section 2.4.

2.2 Friction Models and its Properties

It is well known that friction depends on both velocity and position, but its structure is not well defined, especially at low velocity. For ease of analysis and simulation, it is important to have a mathematical model of friction. A friction model should be able to accurately predict the observed friction characteristics, and be simple enough for friction compensation. Friction is a multifaceted phenomenon, and exhibits the well-known classical Coulomb and viscous friction, nonlinearity at low velocity, and elasticity of contact surfaces. In any given circumstance, some features may dominate over others and some features may not be detectable with the available sensing technology. But all these phenomena are present all the time. The use of a more complete friction model will extend the applicability of analytical results and resolve discrepancies that arise in different investigations. While the classical friction models give only the static relationships between velocity and friction force, the most recent friction model, the so-called LuGre model, is a dynamic model with an unmeasureable internal state. In the following, we shall give a list of commonly used friction models that enable simple controller design and computer simulation.

2.2.1 Behavior of Static Friction Models

The static friction models refer to those models that are functions of velocity/ position only, without any internal dynamics. In this subsection, we will not only list the

commonly known classical static friction components, such as stiction, Coulomb etc., and we will also present a neural network friction model which is easy to use to treat the complexity and difficulty in modelling friction.

Static Friction

At zero velocity, the static friction opposes all motion as long as the torque is smaller in magnitude than the maximum stiction force fs, and is usually described by:

$$F = \begin{cases} u, & |u| < f_s \\ f_s \delta(\dot{x}) \operatorname{sgn}(u) & |u| < f_s \end{cases} \tag{2.1}$$

where,

$$\delta(\dot{x}) = \begin{cases} 1, & \dot{x} = 0 \\ 0, & \dot{x} \neq 0 \end{cases}, \quad \operatorname{sgn}(u) = \begin{cases} +1, & u > 0 \\ -1, & u < 0 \end{cases}$$

In actual implemetation, the impulse function can be approximated differently such as triangular or rectangular as in Karnopps's version of stiction. In fact, stiction is not truly a force of friction, but a force of constraint in presliding and behaves likes a spring. For small motion, the elasticity of asperities suggests that the applied forces is approximately proportional to the presliding displacement as follows:

$$F = f_t x \delta(\dot{x}) \tag{2.2}$$

where f_t is the tangential stiffness of the contact, x is the displacement away from equilibrium position and $\delta(\dot{x})$ is used to describe the fact that stiction occurs only

when at rest. At a critical force, breakaway occurs and true sliding begins. Breakaway has been observed to occur at the order of $2-5$ microns in steel junctions and millimeter motions in robots, where the arms act as levers to amplify the micron motion at the gear teeth. Presliding displacement is of interest to control community in extremely high precision positioning. If sensors are not sensitive enough, we are able to observe only common stiction (2.1).

Coulomb friction

It is independent of the area of contact, Coulomb friction always opposes relative motion and is proportional to the normal force of contact. It does not specify the friction from zero velocity. It may be zero or it can take on any vale in the interval between $-f_c$ and f_c, depending on how the sign function is defined as shown in Figure 2.1. Coulomb friction is described by:

$$F = f_c \text{sgn}\,(\dot{x}) \tag{2.3}$$

where $f_c = \mu|f_n|$ with μ being the coefficient of friction and f_n the normal force. Constant f_c is independent of the magnitude of relative velocity.

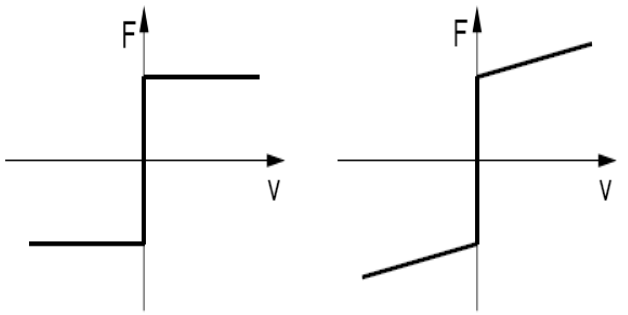

(a) Coulomb friction (b) Coulomb plus viscous friction

Figure 2.1: Static friction models: Coulomb friction and coulomb plus viscous friction (source: [3])

Viscous friction

It corresponds to the well-lubricated situation, and is proportional to velocity. The term viscous friction is used for the force component which is normally described as:

$$F = f_v \dot{x} \tag{2.4}$$

Generally, viscous friction is combined with Coulomb friction as shown in Figure 2.1.

Drag friction

It is caused by resistance to a body moving through a fluid and proportional to the square of velocity as described by:

$$F = f_d |\dot{x}| \dot{x} \tag{2.5}$$

When the speed of travel is small, this term is neglectable. This term cannot be neglected in the control of hard disk drives because of the high speed rotation of spindle motors. Classical friction models have different combitions of Static, Coulomb and Viscous friction as their basic building blocks.

Exponential Model

After reviewing several existing models, an exponential model incorporating Coulomb and Viscous frictions is given as follows:

$$F(\dot{x}) = f_c \text{sgn}(\dot{x}) + (f_s - f_c)\, e^{-(\dot{x}/\dot{x}_s)^{\delta}} + f_v \dot{x} \tag{2.6}$$

where $\dot{x}_S$ and δ are empirical parameters, f_c is Coulomb friction model, f_s is the level of the stiction force and f_v is viscous coefficient. It can be realized by choosing different parameters and different friction as in [47]. While the value of δ is large, Gaussian exponential model is obtained as presented in [48] in the following Gaussian forms.

Gaussian exponential with one break:

$$F(\dot{x}) = f_c \text{sgn}(\dot{x}) + (f_s - f_c)\, e^{-(\dot{x}/\dot{x}_s)^2} + f_v \dot{x} \tag{2.7}$$

Gaussian exponential with two break:

$$F(\dot{x}) = f_c \text{sgn}(\dot{x}) + f_{s_1} e^{-\left(\dot{x}/\dot{x}_{s_1}\right)^2} + F_{s_2} e^{-(\dot{x}/\dot{x}_{s2})^2} + f_v \dot{x} \tag{2.8}$$

Gaussian exponential with two break and offsets:

$$F(\dot{x}) = f_c \text{sgn}(\dot{x}) + f_{s_1} e^{-(\dot{x}-\dot{x}_{10})^2/\dot{x}_{s_1}^2} + F_{s_2} e^{-(\dot{x}-\dot{x}_{10})^2/\dot{x}_{s_2}^2} + f_v \dot{x} \tag{2.9}$$

Tustin's model was obtained when $\delta = 1$ as described in [49]:

$$F(\dot{x}) = f_c \text{sgn}(\dot{x}) + (f_s - f_c)\, e^{-(\dot{x}/\dot{x}_s)} + f_v \dot{x} \tag{2.10}$$

Tustin's model is one of the best models describing friction force at a velocity close to zero. It considers decaying exponential term in the friction model which explains the microscopic limit cycle behavior that has a negative exponential characterization after a breakaway point at $\dot{x}$. It has been proven that this model can approximate real friction forces in [50].

Due to difficulties in dealing with unknown parameter $\dot{x}_s$ in Tustin's model, the following liner-in-parameter (LIP) friction model was proposed in [51].

$$F(\dot{x}) = f_c \text{sgn}(\dot{x}) + f_r \sqrt{\dot{x}} \text{sgn}(\dot{x}) + f_v \dot{x} \tag{2.11}$$

where constant $f_i (i = c, r, v)$ are not unique and depend on the operating velocity. The LIP model is famous because of its own merits such as capturing the downward bends and possible asymmetrics, suitable for on-line identification since its unknown parameters are linear and easy to update changes of these parameters subject to environmental change.

Lorentizian Model

As described in [52], the Lorentzian model has been employed as follows:

$$F(\dot{x}) = f_c \text{sgn}(\dot{x}) + (f_s - f_c) \frac{1}{1 + (\dot{x}/\dot{x}_s)^2} + f_v \dot{x} \tag{2.12}$$

which shows a systematic dependence of $\dot{x}_s$ and f_v on the lubricant and loading parameters. Similar to the case of the Gaussian model, Lorentzian models also have forms with one break, two breaks or two breaks with offsets.

Remark 2.1 *Based on the above discussion, a more complete model may consist of the following components: stiction, Coulomb, viscous and drag friction, and square root friction:*

$$F(x, \dot{x}) = f_t x \delta(\dot{x}) + f_c \text{sgn}(\dot{x}) + f_v \dot{x} + f_d \dot{x} |\dot{x}| + f_r \sqrt{\dot{x}} \text{sgn}(\dot{x}) \tag{2.13}$$

which can be conveniently expressed in LIP form as:

$$F(x, \dot{x}) = S^T(x, \dot{x}) P \tag{2.14}$$

where, $S(x, \dot{x}) = [\delta(\dot{x}), \text{sgn}(\dot{x}), \dot{x}, \dot{x}|\dot{x}|, \sqrt{\dot{x}}\text{sgn}(\dot{x})]^T$, $P = [f_t, f_c, f_v, f_d, f_r]$, in which $S(x, \dot{x})$ is a vector of known basis functions, and P is a vector of unknown parameters.

It is generally considered that friction has two different manifestations, i.e. presliding friction and sliding friction. In the presliding stage, which is usually in the range

of less than 10^{-5}m, friction is dominated by the elasticity of the contacting asperity of surfaces as described by (2.2). It not only depends on both position and velocity of motion, but also exhibits nonlinear dynamic behavior such as hysteresis characteristics with respect to position and velocity as observed by many research works. In the sliding stage, friction is dominated by lubrication of the contacting surface and introduces damping ratio into system. It is usually represented by various functions of velocity. Thus, it can be concluded that friction is continuous though it is highly nonlinear and depends on both position and velocity. Thus, friction can be approximated by neural networks as explained in the following section.

2.2.2 Behaviors of Dynamic Friction Models

All the classical models cannot describe all the dynamic effects of friction such as the presliding displacement, the frictional lag, the Stribeck effect, which all occur in the low velocity and pre-sliding region. Driven by applications with high precision positioning and with low velocity tracking, there has been significant interest in dynamic friction models. In this subsection, several dynamic friction models will be presented.

Dahl Model

The Dahl model introduced in [53] was developed for the purpose of simulating control systems with friction. The starting point for Dahl's model is the stress-strain curve in classical solid mechanics as shown in Figure. (To add figure from Friction Model and

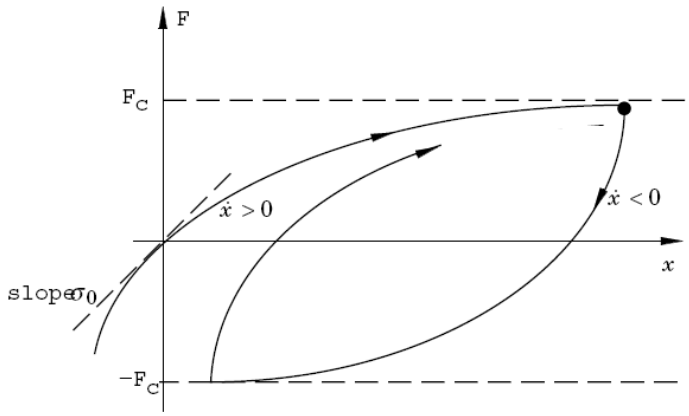

Figure 2.2: Friction force as a function of displacement for Dahl's model (source: [3])

Compensation Paper). When subject to stress the friction force increase gradually until rupture occurs. Let x be the displacement, F is the friction force, and F_c is Coulomb friction force. Dahl's friction model subject to stress-strain curve by a differential equation is obtained the following form.

$$\dot{F} = \sigma \left(1 - \frac{F}{f_c}\text{sgn}\left(\dot{x}\right)\right)^{\alpha} \tag{2.15}$$

where σ is the stiffness coefficient and α is a parameter that determines the shape of the stress-strain curve. The value of $\alpha = 1$ is most commonly used and the higher value of α will give a stress strain curve with a shaper bend. If the initial value is set to $|F| < f_c$, the friction foce $|F|$ will not be larger than $|f_c|$.

The Dhal's model in (2.15) is only a function of the displacement and the sign of the

velocity and its extension can be seen in [54] in the following from:

$$\dot{F} = \sigma \left(1 - \frac{F}{f_c}\text{sgn}\left(\dot{x}\right)\right)^{\alpha} \dot{x} \tag{2.16}$$

The simplified Dahl's model neither captures the Stribecak effect, rate dependent phenomenon, nor does it capture stiction. For the case of $\alpha = 1$, the Dahl model in (2.16) becomes:

$$\dot{F} = \sigma\dot{x} - \frac{F}{f_c}\text{sgn}\left(\dot{x}\right) \tag{2.17}$$

Introducing $F = \sigma z$ the model in (2.17) can be further written as:

$$\dot{z} = \dot{x} - \frac{\sigma\left|\dot{x}\right|}{f_c} z \tag{2.18}$$

$$F = \sigma z \tag{2.19}$$

LuGre Model

The static and dynamic characteristics of friction can be observed in the LuGre model proposed in [55]. The extension of Dahl model can be seen as LuGre model presented in (2.18) and it is modeled as the average deflection of force of elastic springs. The bristle will deflect like springs when a tangential force is applied to the bristles. If the deflection is sufficiently large, the bristles start to slip. The average bristle deflection for a steady state motion is determined by the velocity. It is lower at low velocities, which implies that the steady state deflection decreases with increasing velocity. This models considers the dynamic effects of friction to arise from the deflection of bristles

which model the asperities between two contacting surfaces, and is given by:

$$F = \sigma_0 z + \sigma_1 \dot{z} + \sigma_2 \dot{x} \tag{2.20}$$

$$\dot{z} = \dot{x} - \alpha(\dot{x}) |\dot{x}| z \tag{2.21}$$

where F and z are the friction force and the average deflection of the bristles, which is not measurable, σ_0, σ_1 and σ_2 are friction force parameters that can be physically explained as the stiffness of bristles, damping coefficient and viscous coefficient. $\alpha(\dot{x})$ is a finite positive function which can be chosen to describe different friction effect and is given as follows:

$$\alpha(\dot{x}) = \frac{\sigma_0}{f_c + (f_s - f_c) e^{-(\dot{x}/\dot{x}_s)^2}} \tag{2.22}$$

where f_c, f_s and $\dot{x}_s$ are Coulomb friction force, stiction force and constant Stribeck velocity respectively.

The modified LuGre model is considered in the following form:

$$F = \sigma_0 z + \sigma_1 \dot{z} + \sigma_2 \dot{x} \tag{2.23}$$

$$\dot{z} = \dot{x} - \alpha(x, \dot{x}) |\dot{x}| z \tag{2.24}$$

Remark 2.2 *The model in (2.23) doesn't consider the terms which explicitly account for position dependence of the friction force. However, for some applications that consider LuGre model depends on the actual position, or on a more complex combination of position and velocity in the function, $\alpha(\cdot)$. In the case of dependency on both position and velocity, we assume that $\alpha(x, \dot{x})$ is an upper and lower bounded positive*

smooth function of x *and* $\dot{x}$.

Neural network friction model

Neural networks offer a possible tool for nonlinear mapping approximation. Neural networks can approximate any continuous function to arbitrarily any accuracy over a compact set if the size of the network is large enough. Because of the complexity and difficulty in modelling friction, neural networks may be used to generate input/output maps using the property that a multilayer neural network can approximate any function under mild assumptions with any desired accuracy. It is well known that any sufficiently smooth function can be approximated by a suitably large network suing various activation function, $\sigma(\cdot)$ which include the sigmoid, hyperbolic tangent, radial basis functions, etc. It has been proven that any continuous, not necessarily infinitely smooth, can be uniformly approximated by a linear combinations of Gaussian radial basis function (RBF). The Gaussian RBF neural network is a particular network architecture which uses l Gaussian function of the following form:

$$s_i\left(x,\dot{x}\right)=\exp\left(-\frac{\left(x-\mu_{1i}\right)^2+\left(\dot{x}-\mu_{2i}\right)^2}{\sigma^2}\right),\ i=1,\ldots,l \tag{2.25}$$

where x, $\dot{x}$ are the input variables, σ^2 is the variance and μ_{1i}, μ_{2i} are the centers. A Gaussian RBF neural network can be mathematically expressed as:

$$F_{nn}\left(x,\dot{x}\right)=W^T S\left(x,\dot{x}\right) \tag{2.26}$$

where $S(x, \dot{x}) = [s_1, s_2, \ldots, s_l]^T \in R^l$ is the basis function vector, and $W \in R^l$ is the corresponding weight vector. A general friction model $F_{nn}(x, \dot{x})$ can be written as:

$$F(x, \dot{x}) = F_{nn}(x, \dot{x}) + \varepsilon(x, \dot{x}) \tag{2.27}$$

where $F_{nn}(x, \dot{x})$ is given in (2.26) and $\varepsilon(x, \dot{x})$ is the bounded neural network functional reconstruction error. If there exist integer l and constant weight W such that $\varepsilon = 0$, $F(x, \dot{x})$ is said to be in the functional range of the neural network. For ease of analysis and controller design later, NN-based friction models is investigated in this thesis.

2.3 Choice of Nonlinear Friction Model

In general, the frequency response of the double integrator model is expected to show -40 $db/decade$ slope and $-180°$ phase the the lower end of frequency. However, the frequency response of actuator in Figure 2.3 shows $0db/decade$ slope and $0°$ phase at low frequency range 10-200Hz. On the other hand, it has been stated that the friction force that opposes to the applied force should be a function of both position and velocity. In [35] and [36], it has been discussed that the friction behavior of actuator pivot is not determined by solely by velocity or position, but by a combination of position and velocity.

To describe the friction nonlinearity of actuator pivot in Figure 2.3, it is required to choose a suitable friction model. Several models have been suggested that take feedback of position and velocity into consideration in 2.2. Among them, we choose

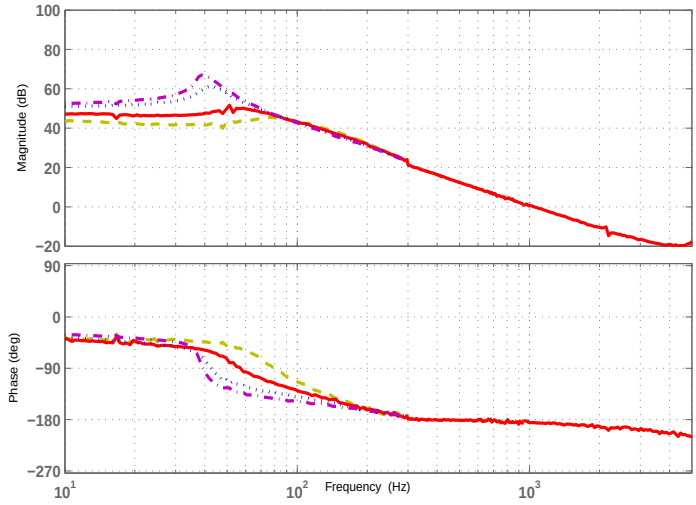

Figure 2.3: Frequency responses of VCM actuator with the influence of friction nonlinearity

LuGre friction model to represent the pivot friction hysteresis nonlinearity in hard disk drive servo system since it's characteristics depends not only on the actual position but also on a combination of position and velocity in the function of $\alpha(\cdot)$ as presented in (2.22). In addition, LuGre friction model introduced in (2.23) possess all the static and dynamic characteristics of hysteresis friction nonlinearity. This model is found to produce very good match between observed response and model response in frequency domain. However, in the time domain hysteresis curve of input voltage versus displacement, the LuGre friction model is quite well match with the actual friction model after carefully selecting different choices of parameter values.

2.4 Conclusion

For high density hard disk drives in mobile applications, PES noise, disk motion, air flow, external vibrations and disturbance and high frequency resonances are all significant factors affecting the speed of and precision of the servo performance. As the existence of friction from pivot nonlinearity can cause large gain reduction in the low frequency range, it will have severe influence especially in HDDs in mobile applications. Therefore, in this thesis, it is desirable to analyze the effect of hysteresis friction for a typical VCM actuator and to provide better suppression of the friction effect in low frequency range without considering and sacrificing the rejection of disturbances and resonances in other frequency range.

Chapter 3

Mathematical Model of Hard Disk Drive Servo System

3.1 Introduction

Generally, there are two ways to obtain plant models such as analytical derivation and system identification in frequency domain. Since the analytical model is developed either by the use of law of nature, knowledge of physics of the plant is essential to work out the model. In system identification the plant is taken as a black box and just only measure its input and output characteristics. Both of these methods will be presented in this chapter.

The organization of this chapter is as follows. The mathematical model of the VCM

actuator and its model with current driver are given in Section 3.2. To obtain a transfer function model, frequency domain identification algorithm and are presented in Section 3.3 before the conclusion is followed in Section 3.4.

3.2 Analytical Derivation of HDD Actuator

The head positioning servo system is an electromechanical system which composed of Voice Coil Motor (VCM) actuator and the amplifier for injecting the current into the coil of VCM. An electromagnetic force is experienced when a current flow through a coil of VCM. Since the actuator arm is attached to the suspended coil and it is pivoted subject to rotating torque. The movement of VCM is driven by current or voltage amplifier. The current amplifier is most widely used in today hard disk drives due to its higher output impedance. The transfer functions or state space representations of the model based on current amplifier are given the following section.

3.2.1 Modeling of VCM actuator

Figure 3.1 shows the architecture of VCM actuator which is the only one component to produce the torque in head positioning servo mechanism. When current is passed through the coil of VCM suspended in the magnetic field produced by permanent magnets, a force (torque) is generated. The generated force (torque) is proportional to coil current and it can be controlled by changing the amplitude and polarity of

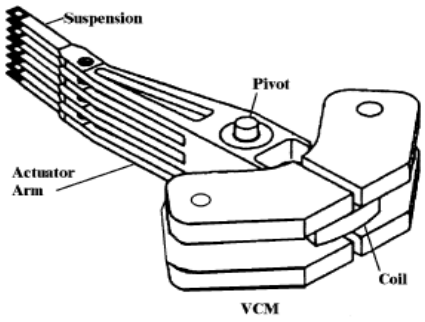

Figure 3.1: VCM actuator (source: [1])

current. In general, there are two types of VCM actuators such as Linear VCM and rotary VCM, in which the rotary actuator is widely used in today hard disk drives due to its smaller size. The torque of rotary actuator given in [13] is presented as follows:

The torque, τ for rotary actuator is given by:

$$\tau = B_g l_{coil} I_m d \tag{3.1}$$

where B_g is a gap flux density; l_{coil} is the length of coil wire cutting the gap flux density; I_m is the coil current of VCM; d is the distance from the bearing to the center of the force; k_t is the torque constant which is defined as:

$$k_t = B_g l_{coil} d \tag{3.2}$$

From 3.1 and 3.2, we obtained:

$$\tau = k_t I_m \tag{3.3}$$

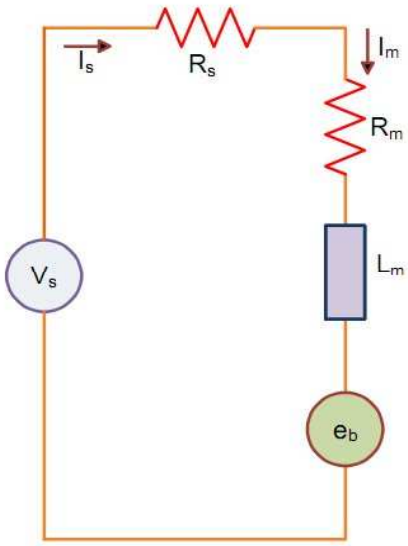

Figure 3.2: The model of VCM actuator

The equation of motion for rotary actuator is given by:

$$\tau = J\ddot{\theta} \tag{3.4}$$

where J is the movement of inertia of the moving parts and θ is angular displacement.

The circuit of VCM model is given in Figure 3.2 and the governing voltage equation of VCM with resistance R and inductance L_m in series is given by:

$$e\,(t) = R_m I_m + L_m \frac{dI_m}{dt} + e_b \tag{3.5}$$

where e is the supply source; R_m and L_m are resistance and inductance of VCM; e_b is the back emf force which is defined as follows with coefficient k_b:

$$e_b = k_b \frac{d\theta}{dt} \tag{3.6}$$

Since the VCM is a DC motor, which needs to be powered by a driver. Since most of currently used VCM are driven by the current drives, the model for the VCM with a current driver will be presented in the next section.

3.2.2 Modeling of VCM actuator with a Current Driver

The disk drive servo is an electromechanical sytem comprising of a VCM and power amplifiers. The VCM driver can be either a voltage or current amplifier as shown in Figure 3.3 and 3.4. The most widely used VCM drivers are current drivers and the analytical model for the VCM with current driver will calculated in this section. According to Figure 3.3 a current driver is considered as a current source plus a resistance and the electrical dynamics of the circuit is given by:

$$\left(I_s - I_m\right) R_s = R_m I_m + L_m \frac{dI_m}{dt} + k_b \frac{d\theta}{dt} \tag{3.7}$$

From 3.3 and 3.4, the mechanical dynamics of the actuator is considered as follows:

$$I_m = \frac{J\ddot{\theta}}{k_t} \tag{3.8}$$

Substituting 3.8 into 3.7, we obtained:

$$I_s = \frac{L_m J}{k_t R_s}\ddot{\theta} + \frac{\left(R_m + R_s\right) J}{k_t R_s}\ddot{\theta} + \frac{k_b}{R_s}\dot{\theta} \tag{3.9}$$

After taking Laplace transform, eq. 3.9 becomes:

$$I_s\left(s\right) = \left[\frac{L_m J}{k_t R_s} s^3 + \frac{\left(R_m + R_s\right) J}{k_t R_s} s^2 + \frac{k_b}{R_s} s\right] \theta\left(s\right) \tag{3.10}$$

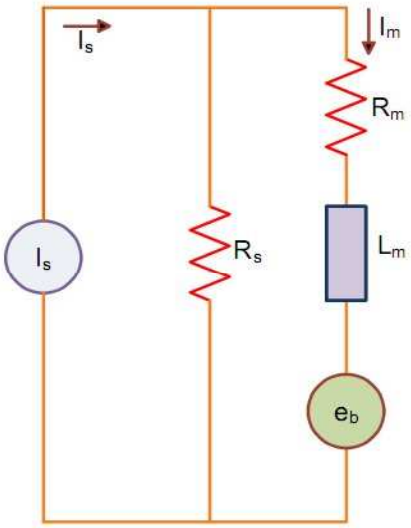

Figure 3.3: The model of VCM actuator with current driver

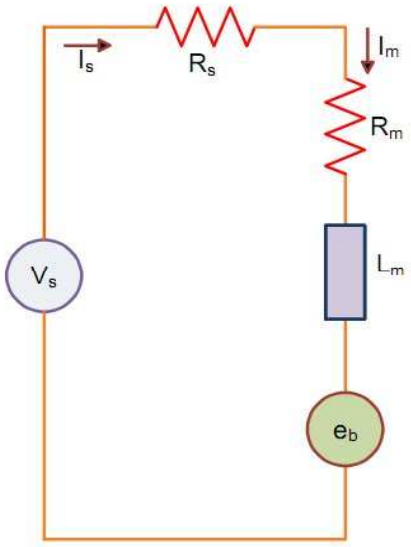

Figure 3.4: The model of VCM actuator with voltage driver

Since $R_s >> R_m$ 3.10 becomes:

$$\frac{\theta(s)}{I_s(s)} = \frac{1}{\frac{k_b}{R_m} s \left[\frac{L_m J R_m}{k_t k_b (R_m + R_s)} s^2 + \frac{R_m J}{k_t k_b} s + \frac{R_m}{R_m + R_s}\right]} \tag{3.11}$$

The plant transfer function in 3.11 becomes as follows:

$$\frac{\theta(s)}{I_s(s)} = \frac{R_m/k_b}{s(s\tau_e + 1)\left[s\tau_m + \frac{R_m}{R_m + R_s}\right]} \tag{3.12}$$

where, the mechanical time constant τ_m and the electrical time constant τ_e is defined as:

$$\tau_m = \frac{R_m J}{k_t k_b}, \quad \tau_e = \frac{L_m}{R_m + R_s} \tag{3.13}$$

As R_s is much larger than R_m, the above transfer function has a pole that is very close to the origin of S-plane. The configuration of VCM driver is presented in Figure 3.3 and the transfer function of amplifier can be simplified as follows:

$$\frac{I_s(s)}{u(s)} = \frac{k_a}{s\tau_a + 1} \tag{3.14}$$

where k_a is the steady state gain; τ_a is the time constant of the amplifier, and u is the voltage input to amplifier.

Thus, the overall transfer function, VCM plant with its current driver becomes:

$$\frac{\theta(s)}{u(s)} = \frac{\frac{R_m k_a}{k_b}}{s(s\tau_e + 1) + (s\tau_a + 1)\left[s\tau_m + \frac{R_m}{(R_m + R_s)}\right]} \tag{3.15}$$

Since τ_a and τ_e are extremely small compared to τ_m and $R_s >> R_m$. Substituting τ_m from 3.13 into 3.15, we obtained:

$$\frac{\theta(s)}{u(s)} = \frac{k_t k_a}{J} \frac{1}{s^2} \tag{3.16}$$

where the voltage input, $u(s)$ to amplifier is the same as the control input to the plant; $\theta(s)$ the position of actuator which is given in radian and it can be transformed to tracks as follows:

$$G(s) = \frac{y(s)}{u(s)} = \left(\frac{k_t k_a}{J}\right)\left(l_{arm}\frac{TPI}{0.0254}\right)\frac{1}{s^2} = k_v k_y \frac{1}{s^2} \tag{3.17}$$

where $k_v = \frac{k_t k_a}{J}$ is defined as the accelreation constant; $k_y = l_{arm}\frac{TPI}{0.0254}$ is named as the position measurement gain; l_{arm} is the length of actuator arm and TPI represent Track Per Inch of rigid body model in hard disk drive.

The state space model of the actuator can be obtained in the following forms:

$$\begin{bmatrix} \dot{y} \\ \dot{v} \end{bmatrix} = \begin{bmatrix} 0 & k_y \\ 0 & 0 \end{bmatrix}\begin{bmatrix} y \\ v \end{bmatrix} + \begin{bmatrix} 0 \\ k_v \end{bmatrix} u \tag{3.18}$$

where the control input u is $|u| \leq u_{\max}$.

3.2.3 Analytical Obtained HDD Actuator Model with Resonances

The actuator and HDD structures are not perfectly rigid and have hundreds of flexible modes which give rise to vibrations and resonances effects. In modern hard disk drives, resonances or vibrations modes are major sources of TMR and it cannot be neglected due to its longer settling time at the targeted track. Even though the simplified transfer function in 3.16 is a double integrator model, the structural resonance effects cannot be ignored due to the high performance requirements in modern hard disk

drive systems. To obtain more accurate model of HDDs, the rigid body model in 3.16 with resonant modes will be described in this section.

Let consider a second order plant model as follows:

$$R(s) = \frac{\omega_n^2}{s^2 + 2\xi_n\omega_n s + \omega_i^2} \tag{3.19}$$

where $\omega_n = 2\pi f_n$ is the natural frequency of the resonant mode which corresponds to a single resonance frequency f; ξ_n is the associated damping coefficient and it is lightly damped as $0.005 \leq \xi_n \leq 0.5$.

A typical plant Bode plot for the disk drive actuator is shown in Figure 1.5. The VCM actuator model containing only one lightly damped resonant mode can be modeled as follows:

$$\begin{aligned} \frac{y(s)}{u(s)} &= G(s)\,R(s) \\ &= \frac{k_y k_v}{s^2}\frac{\omega_n^2}{s^2 + 2\xi_n\omega_n s + \omega_n^2} \\ &= \frac{K}{s^2}\frac{\omega_n^2}{s^2 + 2\xi_n\omega_n s + \omega_n^2} \end{aligned} \tag{3.20}$$

where $R(s)$ is the resonance transfer function defined in (3.19), K is the plant gain, ω_n is the natural frequency and ξ_n is the corresponding ratio.

3.3 Frequency Domain IdentificationAlgorithm

In this section, we present some basic theory of system identification which is to be used in modeling the VCM actuators in HDD servo system in the forthcoming chapter.

The goal of system identification is to determine a mathematical model for a system based on experimental verification data. A large verity of methods have been developed to determine a system model in either time or frequency domain. These methods include classical identification techniques such as the impulse response analysis, step response analysis, frequency response identification and equation error approaches and model adjustment techniques such as the lest square estimation, maximum likeihood and stochastic approximation as in [2]. We restrict our attention to describe system identification algorithm in the frequency domain. The present algorithm is based on the principle of least-square fit on the complex plane and it fits the frequency response data to the response of a transfer function model, minimizing the sum of square of residual errors. Thus a transfer function model is extracted from the measurement of the frequency response at a discrete set of frequencies while the order of the transfer function model is obtained from least-square estimation for different orders of the transfer function.

The detail procedure of frequency response identification method in [56] is given as follows. Suppose that the transfer function of a plant with m^{th} order in s-domain is:

$$G(s) = \frac{N(s)}{D(s)} = \frac{b_n s^n + b_{n-1} s^{n-1} + \cdots + b_0}{a_m s^m + a_{m-1} s^{m-1} + \cdots + a_0} \tag{3.21}$$

where $[b_n, \cdots, b_0]$ and $[a_m, \cdots, a_0]$ are real number and $n \leq m$.

At certain frequency ω_k, the input signal and the output data becomes $X(j\omega_k)$ and $Y(j\omega_k)$ respectively.

$$G\left(j\omega_k\right)=\frac{Y\left(j\omega_k\right)}{X\left(j\omega_k\right)}=\frac{b_n\left(j\omega_k\right)^n+b_{n-1}\left(j\omega_k\right)^{n-1}+\cdots+b_0}{a_m\left(j\omega_k\right)^m+a_{m-1}\left(j\omega_k\right)^{m-1}+\cdots+a_0} \tag{3.22}$$

The parameter $[b_n,\cdots,b_0]$ and $[a_m,\cdots,a_0]$ can be obtained by minimizing the following estimated error equation:

$$\sum_{k=1}^{i}W_k\left\|\frac{N\left(j\omega_k\right)}{D\left(j\omega_k\right)}-\frac{Y\left(j\omega_k\right)}{X\left(j\omega_k\right)}\right\|^2 \tag{3.23}$$

where i is the number of sample data and W_k is a weighting function to put emphasis on certain frequency range. The nonlinear least-square problem can be transformed to a linear optimization problem if we define:

$$\begin{aligned} W_k &= D\left(j\omega_k\right) \\ \frac{Y\left(j\omega_k\right)}{X\left(j\omega_k\right)} &= R\left(j\omega_k\right)+jI\left(j\omega_k\right) \end{aligned} \tag{3.24}$$

The following modified error norm is obtained for minimization:

$$J=\sum_{k=1}^{i}\left\|N\left(j\omega_k\right)-D\left(j\omega_k\right)\left(R\left(\omega_k\right)+j\left(\omega_k\right)\right)\right\|^2 \tag{3.25}$$

The modified error norm can be solved by finding $\hat{a}_i$ and $\hat{b}_j$ such that

$$\frac{\partial J}{\partial a_i}\left|a_i=\hat{a}_i\right.,\quad \frac{\partial J}{\partial b_i}\left|b_i=\hat{b}_i\right. \tag{3.26}$$

where $\partial^2 J/\partial a_i^2>0,\quad \partial^2 J/\partial b_i^2>0.$

3.4 Conclusion

Both analytical derivation and system identification algorithm in frequency domain are presented in this chapter. The mathematical model of hard disk drive system are given based on the rigid body model of VCM with current driver. In addition, an algorithm identifying transfer function model in frequency domain are also given in this chapter. The method is used to identify the model of VCM actuator used in the hard disk drives. According to the model obtained in this chapter, the design of corresponding controller are developed in the forthcoming chapter.

Chapter 4

Adaptive Neural Network Control Control Design

4.1 Introduction

The ever increasing demand for HDDs with higher track density and faster access speeds has given a great challenge for the servo control engineers. The nonlinearity introduced by the pivot friction is among the main factors that limit the servo bandwidth and positioning accuracy. The pivot friction nonlinearity is defined as the friction hysteresis that occurs at the bearing of the actuator pivot in the hard disk drives. In hard disk drive system, as can be seen in Figure 4.1, the R/W head is mounted on an actuator assembly which is supported by a pivot bearing cartridge consisting of a pair of preloaded ball bearings as detailed in Figure 1.6. The balls

within the bearing would swing in certain positions when the actuator oscillate. The hysteresis behavior can be observed in the friction vs displacement plot where the friction torque would not jump instantaneously in step with the reversal of the rotational direction as presented in Figure 5.5 and Figure 5.6.

This nonlinear friction effect can be seen as a large gain reduction gain reduction especially in low frequency range. It can be observable that the presence of friction in the actuator pivot bearing results in large residual errors and high frequency oscillations which may produce larger positioning error signal to hold back the further decreasing of the track width and to deteriorate the performance of the servo systems. The nonlinear friction is much more severe in the track following stage when the R/W head is moving from the current track to its neighborhood tracks. This issue becomes more noticeable for small drives and is one of the challenges to design head positioning servo systems for small HDDs. The desire to fully understand the behavior of nonlinearities and friction in the servo systems is obvious. This desire motivates us to carry out a study and modeling of pivot friction nonlinearity for the VCM actuated HDD servo systems.

As presented in Section 1.3.3, much efforts have been put into the research on mitigation of the friction in the pivot bearing in the HDD industry in the last decade and it is still ongoing in the disk-drive industry. Linear techniques used to suppress the influences by rasing low frequency gain have inherent limitations characterized by the Bode's gain-phase relationship, while model-based techniques relied heavily on

Figure 4.1: Overview of HDD with actuator assembly (source: [4])

the accuracy of the model and lacked of robustness against the unmodelled dynamics and various characteristics. Therefore, it is desirable to provide better suppression of pivot friction nonlinearity by designing an adaptive NN controller which can give a fast convergence of the parameter estimation and improvement in tracking error convergence to a neighborhood of zero.

4.2 Problem Formulation and Preliminaries

Throughout this paper, $\tilde{(\cdot)} = \hat{(\cdot)} - (\cdot)$; $\|\cdot\|$ denotes the 2-norm; $\lambda_{\min}(\cdot)$ and $\lambda_{\max}(\cdot)$ denote the smallest and largest eigenvalues of a square matrix $(\cdot)$, respectively.

4.2.1 Dynamics of Hard Disk Drive System

Consider the following voice-coil-motor (VCM) actuator dynamics with the hysteresis friction nonlinearity:

$$m\ddot{x} + h(x, \dot{x}) + d(t) = u \tag{4.1}$$

where m is an unknown system constant, which models the system inertial mass; x, $\dot{x}$ and $\ddot{x}$ are the position, velocity and acceleration of VCM actuator read/write (R/W) head tip respectively; $d(t)$ is the external disturbance; u is the control input; $h(x, \dot{x})$ is the bearing hysteresis friction of actuator pivot, which is represented as a LuGre friction model consisting of stiffness and viscous friction behaviors as follows [46][33]:

$$h = \sigma_0 z + \sigma_1 \dot{z} + \sigma_2 \dot{x} \tag{4.2}$$

$$\dot{z} = \dot{x} - \alpha(\dot{x}) |\dot{x}| z \tag{4.3}$$

$$\alpha(\dot{x}) = \frac{\sigma_0}{f_c + (f_s - f_c) e^{-(\dot{x}/\dot{x}_s)^2}} \tag{4.4}$$

where z denotes an unmeasurable internal state of the friction model; σ_0, σ_1 and σ_2 are the hysteresis friction force parameters that can be physically explained as the stiffness of bristles, damping coefficient, and viscous coefficient; f_c, f_s and $\dot{x}_s$ are the Coulomb friction, static friction and Stribeck velocity respectively; and the nonlinear friction characteristic function $\alpha(\dot{x})$ is a bounded positive function which can be chosen to describe different friction effects.

Remark 4.1 *Note that there are no terms which explicitly account for the position*

dependence of the hysteresis friction force in the above model (4.2)-(4.4). However, there may exist some applications where the function $\alpha(\cdot)$ in the LuGre model also depends on the actual position, or on a more complex combination of position and velocity. Therefore, we assume that $\alpha(x, \dot{x})$ is an upper and lower bounded positive smooth function of x and $\dot{x}$, and consider the LuGre model in the following form:

$$h = \sigma_0 z + \sigma_1 \dot{z} + \sigma_2 \dot{x} \tag{4.5}$$

$$\dot{z} = \dot{x} - \alpha(x, \dot{x})|\dot{x}|z \tag{4.6}$$

Remark 4.2 *Figure 5.5 shows that the dynamic equations (4.1)-(4.4) can indeed generate the hysteresis friction nonlinearity curve, where the parameters are chosen as stated in Section 5.4. Recognizing the very fact that realistic accurate hysteresis friction nonlinearity model building or parameter identification might be more difficult or complicated in practice than controller design, we adopt neural networks in control design to handle the hysteresis nonlinearity and mitigate its effect on the tracking performance.*

The control objective is to ensure that the position of the VCM actuator read/write (R/W) head tip x follows the specified desired trajectory x_d to a small neighborhood of zero.

To facilitate control design later in Section 4.3, we need the following assumptions:

Assumption 4.1 *The desired trajectories, x_d, and its first and second derivatives, $\dot{x}_d$ and $\ddot{x}_d$, are bounded and continuous signals.*

Assumption 4.2 *The external disturbance $d(t)$ satisfies the following condition:*

$$|d(t)| \leq d^*$$

where d^* is an unknown positive constant.

Assumption 4.3 *There exist positive constants α_{min} and α_{max} such that $0 < \alpha_{min} \leq \alpha(x, \dot{x}) \leq \alpha_{max}$, $\forall (x, \dot{x}) \in R^2$.*

Remark 4.3 *According to (4.4) and Remark 4.1, Assumption 4.3 is valid.*

The following lemma will be used in our design and analysis.

Lemma 4.1 *[46] Noting Assumption 4.3, if $|z(0)| \leq 1/\alpha_{min}$, then $|z(t)| \leq 1/\alpha_{min}$, $\forall t \geq 0$.*

4.2.2 Function Approximation Using Radial Basis Function Neural Network

In control engineering, radial basis function neural network (RBFNN) has been successfully used as a linearly parameterized function approximator to unknown functions

due to its good capabilities [57][58]. The RBFNN can be used to approximate the continuous function $f(Z) : R^m \rightarrow R$ as follows:

$$f(Z) = W^T S(Z) + \varepsilon(Z) \tag{4.7}$$

where the input vector $Z \in \Omega_Z \subset R^m$; weight vector $W = [w_1, w_2, ..., w_l]^T \in R^l$, the NNs node number $l > 1$; $S(Z) = [s_1(Z), ..., s_l(Z)]^T$, with $s_i(Z)$ being chosen as the commonly used Gaussian functions, which have the form

$$s_i(Z) = \exp\left[\frac{-(Z-\mu_i)^T(Z-\mu_i)}{\eta_i^2}\right], \quad i = 1, 2, ..., l$$

where $\mu_i = [\mu_{i1}, \mu_{i2}, ..., \mu_{im}]^T$ is the center of the receptive field and η_i is the width of the Gaussian function; and $\varepsilon(Z)$ is the approximation error which is bounded over the compact set Ω_Z, i.e., $|\varepsilon(Z)| \leq \bar{\varepsilon}$, $\forall Z \in \Omega_Z$ where $\bar{\varepsilon} > 0$ is an unknown constant.

It has been proven that RBFNN (4.7) can approximate any continuous function $f(Z)$ over a compact set $\Omega_Z \subset R_m$ to arbitrary any degree of accuracy as

$$f(Z) = W^{*T} S(Z) + \varepsilon^*(Z), \quad \forall Z \in \Omega_Z \subset R^m \tag{4.8}$$

where W^* is ideal constant weights, and $\varepsilon^*(Z)$ is the approximation error for the special case where $W = W^*$.

Assumption 4.4 *On the compact set Ω_Z, the ideal NN weights W^* is bounded by*

$$\|W^*\| \leq w_m \tag{4.9}$$

The ideal weight vector W^* is defined as the value of W that minimizes $|\varepsilon(Z)|$ for all $Z \in \Omega_Z \subset R^m$, i.e.,

$$W^* = \arg\min_{W}\{\sup_{Z\in\Omega_Z} |f(Z) - W^T S(Z)|\}$$

In general, the ideal weights W^* are unknown and need to be estimated in control design. Let $\hat{W}$ be the estimates of W^* , and the weight estimation errors $\tilde{W} = \hat{W} - W^*$.

Remark 4.4 *Although RBFNN is employed in our control design, it can be replaced by other linearly parameterized function approximators such as high-order neural networks, fuzzy systems, polynomials, splines and wavelet networks without difficulty.*

4.3 Control Design and Stability Analysis

In this section, we will design adaptive control for the plant (4.1)(4.5)(4.6) to achieve the tracking objective.

Define the tracking error e and the filtered tracking error r as follows:

$$e = x - x_d, \quad r = \dot{e} + \lambda e \tag{4.10}$$

where $\lambda > 0$ is a design parameter.

Define the reference velocity and acceleration signals as follows:

$$\dot{x}_r = \dot{x}_d - \lambda e, \quad \ddot{x}_r = \ddot{x}_d - \lambda \dot{e} \tag{4.11}$$

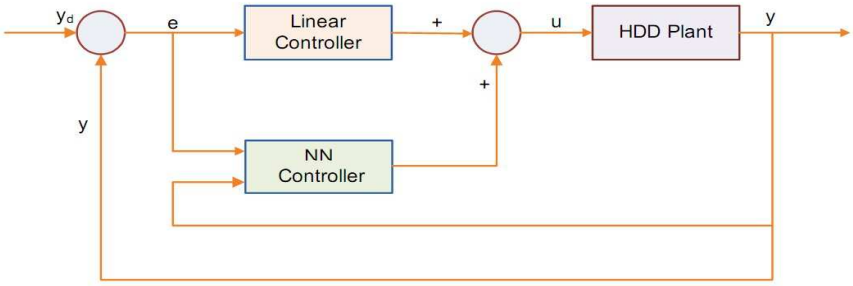

Figure 4.2: Block diagram of proposed friction compensator with neural network

Substituting (4.6) into (4.5), we obtain

$$\begin{aligned} h &= \sigma_1\dot{x} + \sigma_2\dot{x} + \sigma_0 z - \sigma_1\alpha(x,\dot{x})|\dot{x}|z \\ &= \sigma\dot{x} + h_z(x,\dot{x},z) \end{aligned} \tag{4.12}$$

where $\sigma = \sigma_1 + \sigma_2$, and $h_z(x,\dot{x},z) = \sigma_0 z - \sigma_1\alpha(x,\dot{x})|\dot{x}|z$, which depends on z.

From Lemma 4.1, we know that h_z is bounded by

$$\begin{aligned} |h_z(x,\dot{x},z)| &= |(\sigma_0 - \sigma_1\alpha(x,\dot{x})|\dot{x}|)||z(t)| \\ &\leq \frac{\sigma_0 + \sigma_1\alpha(x,\dot{x})|\dot{x}|}{\alpha_{min}} = \bar{h}_z(x,\dot{x}) \end{aligned} \tag{4.13}$$

where $\bar{h}_z(x,\dot{x})$ is the bounding function of $h_z(x,\dot{x},z)$ and is independent of the unmeasurable internal state z.

Remark 4.5 *From (4.12) and (4.13), we know that the dynamic hysteresis friction model in (4.12) can be separated into two parts: (i) the term $\sigma\dot{x}$ with unknown constant coefficient, and (ii) the term $h_z(x,\dot{x},z)$ which is a function of the unmeasurable internal state $z(t)$ and is bounded by a function which is independent of $z(t)$.*

Then, we use radial basis function neural network (RBFNN) in Section 4.2.2 to approximate the unknown bounding function $\bar{h}_z(x, \dot{x})$ as

$$\bar{h}_z(x, \dot{x}) = W^{*T} S(x, \dot{x}) + \epsilon(x, \dot{x}) \tag{4.14}$$

where W^* is the optimal weight vector, and $\epsilon(x, \dot{x})$ is the NN approximation error, which satisfies $|\epsilon(x, \dot{x})| \leq \epsilon^*, \quad \forall (x, \dot{x}) \in \Omega$, with a positive constant ϵ^*.

Let us consider the following quadratic function $V_r = \frac{1}{2} m r^2$. According to (4.1), (4.10)-(4.14), the derivative of V_r can be written as

$$\begin{aligned}
\dot{V}_r &= mr\dot{r} \\
&= r[u - \sigma\dot{x} - h_z(x, \dot{x}, z) - d(t) - m\ddot{x}_r] \\
&= r[u - \sigma\dot{x} - m\ddot{x}_r] - r[h_z(x, \dot{x}, z) + d(t)] \\
&\leq r[u - \sigma\dot{x} - m\ddot{x}_r] + |r|[\bar{h}_z(x, \dot{x}) + d^*] \\
&\leq r[u - \sigma\dot{x} - m\ddot{x}_r] + |r|[W^{*T} S(x, \dot{x}) + \phi]
\end{aligned} \tag{4.15}$$

where $\phi = \epsilon^* + d^*$.

Consider the following control

$$u = -kr + \hat{\sigma}\dot{x} + \hat{m}\ddot{x}_r - \hat{W}^T S(x, \dot{x})\text{sgn}(r) - \hat{\phi}\text{sgn}(r) \tag{4.16}$$

where constant $k > 0$, $\hat{\sigma}$, $\hat{m}$ and $\hat{\phi}$ are the estimates of unknown parameters σ, m and ϕ respectively.

Substituting (4.16) into (4.15) leads to

$$\dot{V}_r \leq -kr^2 + \tilde{\sigma}\dot{x}r + \tilde{m}\ddot{x}_r r - \tilde{W}^T S(x,\dot{x})|r| - \tilde{\phi}|r| \tag{4.17}$$

Theorem 4.1 *Consider the closed-loop system consisting of system (4.1) with dynamic hysteresis friction given by (4.5) and (4.6), and the control law (4.16). If the Assumptions 4.1-4.3 are satisfied and the parameters $\hat{\sigma}$, $\hat{m}$, $\hat{\phi}$ and NN weight $\hat{W}$ are updated by*

$$\dot{\hat{\sigma}} = -k_\sigma(\dot{x}r + \sigma_\sigma\hat{\sigma}) \tag{4.18}$$

$$\dot{\hat{m}} = -k_m(\ddot{x}_r r + \sigma_m\hat{m}) \tag{4.19}$$

$$\dot{\hat{\phi}} = k_\phi(|r| - \sigma_\phi\hat{\phi}) \tag{4.20}$$

$$\dot{\hat{W}} = \Gamma[S(x,\dot{x})|r| - \sigma_w\hat{W}] \tag{4.21}$$

where k_σ, k_m, k_ϕ, σ_σ, σ_m and σ_ϕ are positive design constant parameters, $\Gamma = \Gamma^T > 0$ is a dimensionally compatible constant matrix, then given any initial compact set defined by

$$\Omega_0 = \Big\{x(0), x_d(0), \hat{\theta}(0), \hat{m}(0), \hat{\phi}(0), \hat{W}(0)\Big| x(0), \hat{\theta}(0), \hat{m}(0), \hat{\phi}(0), \hat{W}(0) \text{ are chosen } finite, x_d(0) \in \Omega_d\Big\}$$

(i) *All the closed loop signals will be remained in a compact set which is given by:*

$$\Omega = \Big\{e, x, \hat{\sigma}, \hat{m}, \hat{\phi}, \hat{W}\Big| |e| \leq |e(0)| + \frac{1}{\lambda}\sqrt{\frac{2V(0) + \frac{2c_2}{c_1}}{m}}$$
$$|x| \leq \max_{[0,t]}|x_d| + |e(0)| + \frac{1}{\lambda}\sqrt{\frac{2V(0) + \frac{2c_2}{c_1}}{m}},$$

$$|\hat{\sigma}| \leq |\sigma| + \sqrt{(2V(0) + \frac{2c_2}{c_1})k_\sigma}, \;\; |\hat{m}| \leq |m| + \sqrt{(2V(0) + \frac{2c_2}{c_1})k_m},$$
$$|\hat{\phi}| \leq |\phi| + \sqrt{(2V(0) + \frac{2c_2}{c_1})k_\phi}, \;\; \|\hat{W}\| \leq \|W^*\| + \sqrt{\frac{2V(0) + \frac{2c_2}{c_1}}{\lambda_{\min}(\Gamma^{-1})}}\Big\}$$

(ii) *All the closed loop signals will eventually converge to the compact sets which is defined by:*

$$\begin{aligned}\Omega_s \;=\; & \Big\{e, x, \hat{\sigma}, \hat{m}, \hat{\phi}, \hat{W}\Big| \lim_{t\to\infty}|e| = \frac{1}{\lambda}\sqrt{\frac{2c_2}{mc_1}}, \quad \lim_{t\to\infty}|x| = \max_{[0,t]}|x_d| + \frac{1}{\lambda}\sqrt{\frac{2c_2}{mc_1}}, \\ & \lim_{t\to\infty}|\hat{\sigma}| = |\sigma| + \sqrt{\frac{2c_2k_\sigma}{c_1}}, \quad \lim_{t\to\infty}|\hat{m}| = |m| + \sqrt{\frac{2c_2k_m}{c_1}}, \\ & \lim_{t\to\infty}|\hat{\phi}| = |\phi| + \sqrt{\frac{2c_2k_\phi}{c_1}}, \quad \lim_{t\to\infty}\|\hat{W}\| = \|W^*\| + \sqrt{\frac{2c_2}{\lambda_{\min}(\Gamma^{-1})c_1}} \quad .\end{aligned}$$

In particular, the tracking error will converge to a neighborhood of zero by adjusting some control design parameters.

Proof: Consider the following Lyapunov function candidate:

$$V = V_r + \frac{1}{2k_\sigma}\tilde{\sigma}^2 + \frac{1}{2k_m}\tilde{m}^2 + \frac{1}{2k_\phi}\tilde{\phi}^2 + \frac{1}{2}\tilde{W}^T\Gamma^{-1}\tilde{W} \tag{4.22}$$

Its derivative along (4.17) is

$$\begin{aligned}\dot{V} \;\leq\; & -kr^2 + \tilde{\sigma}\dot{x}r + \tilde{m}\ddot{x}_r r - \tilde{W}^T S(x,\dot{x})|r| - \tilde{\phi}|r| + \frac{1}{k_\sigma}\tilde{\sigma}\dot{\tilde{\sigma}} + \frac{1}{k_m}\tilde{m}\dot{\tilde{m}} \\ & + \frac{1}{k_\phi}\tilde{\phi}\dot{\tilde{\phi}} + \tilde{W}^T\Gamma^{-1}\dot{\tilde{W}} \\ \leq\; & -kr^2 + \tilde{\sigma}(\dot{x}r + \frac{1}{k_\sigma}\dot{\tilde{\sigma}}) + \tilde{m}(\ddot{x}_r r + \frac{1}{k_m}\dot{\tilde{m}}) + \tilde{\phi}(-|r| + \frac{1}{k_\phi}\dot{\tilde{\phi}}) \\ & + \tilde{W}^T[-S(x,\dot{x})|r| + \Gamma^{-1}\dot{\tilde{W}}]\end{aligned} \tag{4.23}$$

Noticing that $\dot{\tilde{\sigma}} = \dot{\hat{\sigma}}$, $\dot{\tilde{m}} = \dot{\hat{m}}$, $\dot{\tilde{\phi}} = \dot{\hat{\phi}}$, and substituting (4.18)- (4.21) into (4.23), we have

$$\dot{V} \leq -kr^2 - \sigma_\sigma \tilde{\sigma}\hat{\sigma} - \sigma_m \tilde{m}\hat{m} - \sigma_\phi \tilde{\phi}\hat{\phi} - \sigma_w \tilde{W}\hat{W} \tag{4.24}$$

By completion of squares, the following inequalities hold

$$-\sigma_\sigma \tilde{\sigma}\hat{\sigma} \leq -\frac{\sigma_\sigma}{2}\tilde{\sigma}^2 + \frac{\sigma_\sigma}{2}\sigma^2 \tag{4.25}$$

$$-\sigma_m \tilde{m}\hat{m} \leq -\frac{\sigma_m}{2}\tilde{m}^2 + \frac{\sigma_m}{2}m^2 \tag{4.26}$$

$$-\sigma_\phi \tilde{\phi}\hat{\phi} \leq -\frac{\sigma_\phi}{2}\tilde{\phi}^2 + \frac{\sigma_\phi}{2}\phi^2 \tag{4.27}$$

$$-\sigma_w \tilde{W}^T\hat{W} \leq -\frac{\sigma_w}{2}\|\tilde{W}\|^2 + \frac{\sigma_w}{2}\|W^*\|^2 \tag{4.28}$$

Substituting (4.25)-(4.28) into (4.24), we have the following equations:

$$\begin{aligned}\dot{V} &\leq -kr^2 - \frac{\sigma_\sigma}{2}\tilde{\sigma}^2 - \frac{\sigma_m}{2}\tilde{m}^2 - \frac{\sigma_\phi}{2}\tilde{\phi}^2 - \frac{\sigma_W}{2}\|\tilde{W}\|^2 \\ &\quad + \frac{\sigma_\sigma}{2}\sigma^2 + \frac{\sigma_m}{2}m^2 + \frac{\sigma_\phi}{2}\phi^2 + \frac{\sigma_w}{2}\|W^*\|^2 \\ &\leq -c_1 V + c_2 \end{aligned} \tag{4.29}$$

where

$$c_1 = \min\left\{2k, \sigma_\sigma k_\sigma, \sigma_m k_m, \sigma_\phi k_\phi, \frac{\sigma_w}{\lambda_{\max}(\Gamma^{-1})}\right\}, \tag{4.30}$$

$$c_2 = \frac{\sigma_\sigma}{2}\sigma^2 + \frac{\sigma_m}{2}m^2 + \frac{\sigma_\phi}{2}\phi^2 + \frac{\sigma_w}{2}\|W^*\|^2 \tag{4.31}$$

Multiplying (4.29) by $e^{c_1 t}$ yields,

$$\frac{d}{dt}(V(t)e^{c_1 t}) \leq c_2 e^{c_1 t} \tag{4.32}$$

Integrating both sides of (4.32) over $[0, t]$ leads to the following equation:

$$0 \leq V(t) \leq \Big[V(0) - \frac{c_2}{c_1}\Big]e^{-c_1 t} + \frac{c_2}{c_1} \tag{4.33}$$

where

$$V(0) = \frac{1}{2}mr^2(0) + \frac{1}{2k_\sigma}\tilde{\sigma}^2(0) + \frac{1}{2k_m}\tilde{m}^2(0) + \frac{1}{2k_\phi}\tilde{\phi}^2(0) + \frac{1}{2}\tilde{W}^T(0)\Gamma^{-1}\tilde{W}(0) \tag{4.34}$$

(i) Uniform Boundedness (UB)

From (4.33), we have

$$0 \leq V(t) \leq \Big[V(0) - \frac{c_2}{c_1}\Big]e^{-c_1 t} + \frac{c_2}{c_1} \leq V(0) + \frac{c_2}{c_1} \tag{4.35}$$

From (4.22) and (4.35), we have

$$\begin{aligned}
|r| &\leq \sqrt{\frac{2V(0) + \frac{2c_2}{c_1}}{m}}, \\
|\tilde{\sigma}| &\leq \sqrt{(2V(0) + \frac{2c_2}{c_1})k_\sigma}, \\
|\tilde{m}| &\leq \sqrt{(2V(0) + \frac{2c_2}{c_1})k_m}, \\
|\tilde{\phi}| &\leq \sqrt{(2V(0) + \frac{2c_2}{c_1})k_\phi}, \\
\|\tilde{W}\| &\leq \sqrt{\frac{2V(0) + \frac{2c_2}{c_1}}{\lambda_{\min}(\Gamma^{-1})}}
\end{aligned} \tag{4.36}$$

Since $\tilde{\sigma} = \hat{\sigma} - \sigma$, $\tilde{m} = \hat{m} - m$, $\tilde{\phi} = \hat{\phi} - \phi$ and $\tilde{W} = \hat{W} - W^*$, we have

$$\begin{aligned}
|\hat{\sigma}| - |\sigma| &\leq |\hat{\sigma} - \sigma| \leq \sqrt{(2V(0) + \frac{2c_2}{c_1})k_\sigma}, \\
|\hat{m}| - |m| &\leq |\hat{m} - m| \leq \sqrt{(2V(0) + \frac{2c_2}{c_1})k_m}
\end{aligned}$$

$$
\begin{aligned}
|\hat{\phi}| - |\phi| &\leq |\hat{\phi} - \phi| \leq \sqrt{(2V(0) + \frac{2c_2}{c_1})k_\phi}, \\
\|\hat{W}\| - \|W^*\| &\leq \|\hat{W} - W^*\| \leq \sqrt{\frac{2V(0) + \frac{2c_2}{c_1}}{\lambda_{\min}(\Gamma^{-1})}}
\end{aligned} \tag{4.37}
$$

i. e. ,

$$
\begin{aligned}
|\hat{\sigma}| &\leq |\sigma| + \sqrt{(2V(0) + \frac{2c_2}{c_1})k_\sigma}, \\
|\hat{m}| &\leq |m| + \sqrt{(2V(0) + \frac{2c_2}{c_1})k_m} \\
|\hat{\phi}| &\leq |\phi| + \sqrt{(2V(0) + \frac{2c_2}{c_1})k_\phi}, \\
\|\hat{W}\| &\leq \|W^*\| + \sqrt{\frac{2V(0) + \frac{2c_2}{c_1}}{\lambda_{\min}(\Gamma^{-1})}}
\end{aligned} \tag{4.38}
$$

From the definition of r in (4.10), we have

$$
\dot{e} = -\lambda e + r \tag{4.39}
$$

Solving this equation results in

$$
e = \ e^{-\lambda t}e(0) + \int_0^t e^{-\lambda(t-\tau)}|r|d\tau \tag{4.40}
$$

Combining (4.40) with (4.36), the following equation is obtained:

$$
|e| \leq |e(0)| + \frac{1}{\lambda}\sqrt{\frac{2V(0) + \frac{2c_2}{c_1}}{m}} \tag{4.41}
$$

From (4.10), we have

$$
|x| \leq \max_{[0,t]}|x_d| + |e(0)| + \frac{1}{\lambda}\sqrt{\frac{2V(0) + \frac{2c_2}{c_1}}{m}} \tag{4.42}
$$

(ii) Uniformly Ultimate Boundedness (UUB)

From (4.22) and (4.33), we have

$$\begin{aligned}
|r| &\leq \sqrt{\frac{2[V(0)-\frac{c_2}{c_1}]e^{-c_1 t}+\frac{2c_2}{c_1}}{m}},\\
|\tilde{\sigma}| &\leq \sqrt{\Big[2(V(0)-\frac{c_2}{c_1})e^{-c_1 t}+\frac{2c_2}{c_1}\Big]k_\sigma},\\
|\tilde{m}| &\leq \sqrt{\Big[2(V(0)-\frac{c_2}{c_1})e^{-c_1 t}+\frac{2c_2}{c_1}\Big]k_m},\\
|\tilde{\phi}| &\leq \sqrt{\Big[2(V(0)-\frac{c_2}{c_1})e^{-c_1 t}+\frac{2c_2}{c_1}\Big]k_\phi},\\
|\tilde{W}\| &\leq \sqrt{\frac{2[V(0)-\frac{c_2}{c_1}]e^{-c_1 t}+\frac{2c_2}{c_1}}{\lambda_{\min}(\Gamma^{-1})}}
\end{aligned} \tag{4.43}$$

Let us analyze the property of $|r|$ first. If $V(0)=c_2/c_1$, then $|r|\leq\sqrt{\frac{2c_2}{mc_1}}$, $\forall t\geq 0$. If $V(0)\neq c_2/c_1$, from (4.43), we can conclude that given any $\mu_r>\frac{2c_2}{mc_1}$, there exists T_r , such that for any $t>T_r$, we have $|r|\leq\mu_r$. Specially, given any μ_r

$$\mu_r=\sqrt{\frac{2[V(0)-\frac{c_2}{c_1}]e^{-c_1 T_r}+\frac{2c_2}{c_1}}{m}},\quad V(0)\neq\frac{c_2}{c_1}$$

then

$$T_r=-\frac{1}{c_1}\ln\Big(\frac{\mu_e^2 m-\frac{2c_2}{c_1}}{2[V(0)-\frac{c_2}{c_1}]}\Big)$$

and

$$\lim_{t\to\infty}|r|=\sqrt{\frac{2c_2}{mc_1}} \tag{4.44}$$

From (4.40) and (4.44), we obtain that

$$\lim_{t\to\infty}|e|=\frac{1}{\lambda}\sqrt{\frac{2c_2}{mc_1}} \tag{4.45}$$

and

$$\lim_{t\to\infty}|x|=\max_{[0,t]}|x_d|+\frac{1}{\lambda}\sqrt{\frac{2c_2}{mc_1}} \tag{4.46}$$

Similar conclusions can be made about $|\hat{\sigma}|,\ |\hat{m}|,\ |\hat{\phi}|,\ \|\hat{W}\|$ as follows

$$\begin{aligned}
\lim_{t\to\infty} |\hat{\sigma}| &= |\sigma| + \sqrt{\frac{2c_2 k_\sigma}{c_1}}, \\
\lim_{t\to\infty} |\hat{m}| &= |m| + \sqrt{\frac{2c_2 k_m}{c_1}} \\
\lim_{t\to\infty} |\hat{\phi}| &= |\phi| + \sqrt{\frac{2c_2 k_\phi}{c_1}}, \\
\lim_{t\to\infty} \|\hat{W}\| &= \|W^*\| + \sqrt{\frac{2c_2}{\lambda_{\min}(\Gamma^{-1})c_1}}
\end{aligned}$$

From (4.45) and the definitions of c_1 and c_2 in (4.30), we know that the tracking error e can converge to a neighborhood of zero after increasing the parameters $\lambda, k, k_\sigma, k_m, k_\phi, 1/(\lambda_{\max}(\Gamma^{-1}))$, and decreasing $\sigma_\sigma, \sigma_m, \sigma_\phi, \sigma_W$. ■

4.4 Simulation Studies

As presented in [59], to demonstrate the effectiveness of our proposed control design, simulations was performed on the plant model which is described in (4.1),(4.5) and (4.6) under the following choices of the parameter values: $m = 1.0$, $\sigma_0 = 10^5$, $\sigma_1 = \sqrt{10^5}$, $\sigma_2 = 0.4$, $\dot{x}_s = 0.001$, $f_c = 1$, $f_s = 1.5$, $d(t) = 0.1\sin(20t)$. The proposed control is mainly investigated for the purpose of trajectory tracking in which the output x is required to follow the reference trajectory $x_d = \sin(5t)$.

For the neural network $\hat{W}^T S(x, \dot{x})$, the centers for $S(x, \dot{x})$ has been considered to be evenly spaced in a regular lattice in R^2. Employing five nodes for each input dimension, it ends up with $5^2 = 25$ nodes. The design parameters in control (4.16)

and adaption laws (4.18)-(4.21) are chosen as: $\lambda = 1.0, k = 10.0, k_\theta = 1.0, k_\phi = 1.0, k_m = 1.0, \sigma_\theta = 0.1, \sigma_\phi = 0.1, \sigma_m = 0.1$, $\Gamma = diag\{1.0\}$, $\sigma_w = 1.0$. The initial conditions are taken as: $x(0) = \dot{x}(0) = 0.0$, $\hat{W}(0) = 0.0$, $\hat{\theta}(0) = \hat{\phi}(0) = \hat{m}(0) = 0.0$.

The simulation results are detailed in Figs 4.3-4.7. From Fig. 4.3, it can be seen that the tracking performance has been improved compared with conventional PID control. The bounededness of control signals u are shown in Fig. 4.4, while norm of NN weights $\|W\|$, and the estimated parameters $\hat{\theta}$, $\hat{\phi}$ and $\hat{m}$, are shown in Fig. 4.5 and Fig. 4.6, respectively.

To illustrate the effect of parameter λ on the tracking performance, the comparison studies of different λ values are shown in Fig. 4.7. It can be observed that the larger the value of λ, the smaller the tracking errors can be achieved. However, if the λ is chosen too small, the control gain becomes very large, which is not expected in the application. Therefore, there is a compromise between the tracking performance and the control efforts. Here, we recommend that λ is chosen between 0.1 and 15.

4.5 Conclusion

In this chapter, an improved adaptive neural network (NN) controller was designed to compensate for the pivot friction hysteresis nonlinearity. By considering the position and velocity tracking control of a servo mechanism with hysteresis friction, an adaptive NN friction compensation scheme was given based on the dynamic LuGre friction

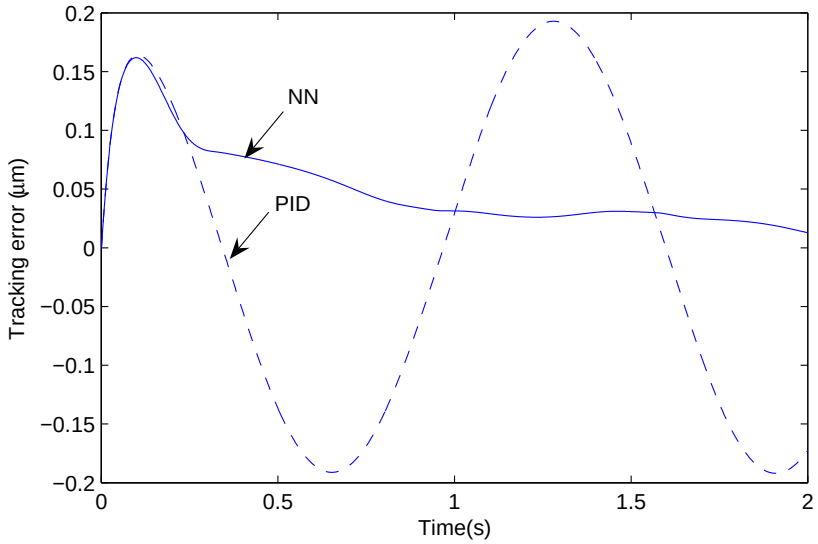

Figure 4.3: Output tracking performance comparison

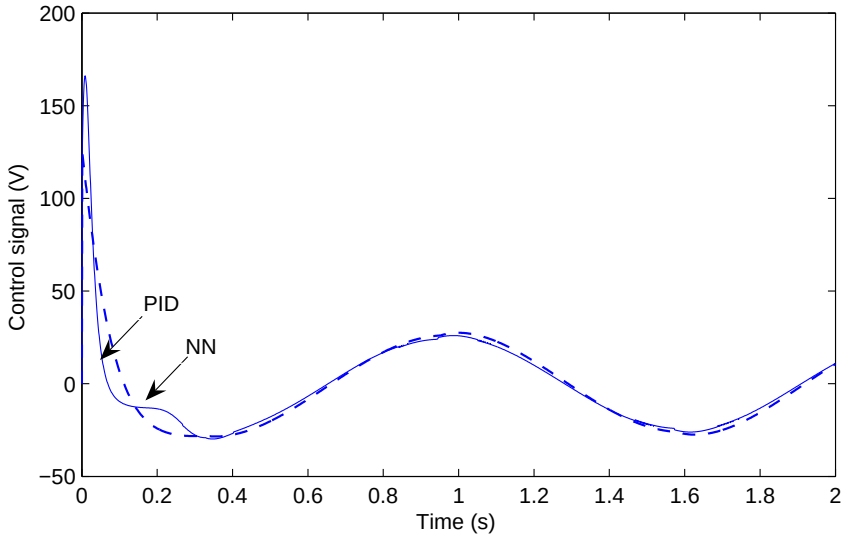

Figure 4.4: Control inputs comparison

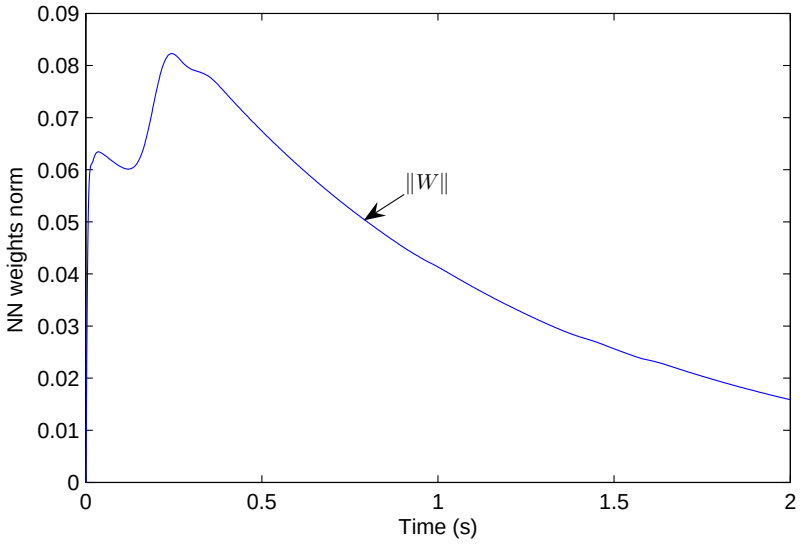

Figure 4.5: NN weights norm $\|W\|$

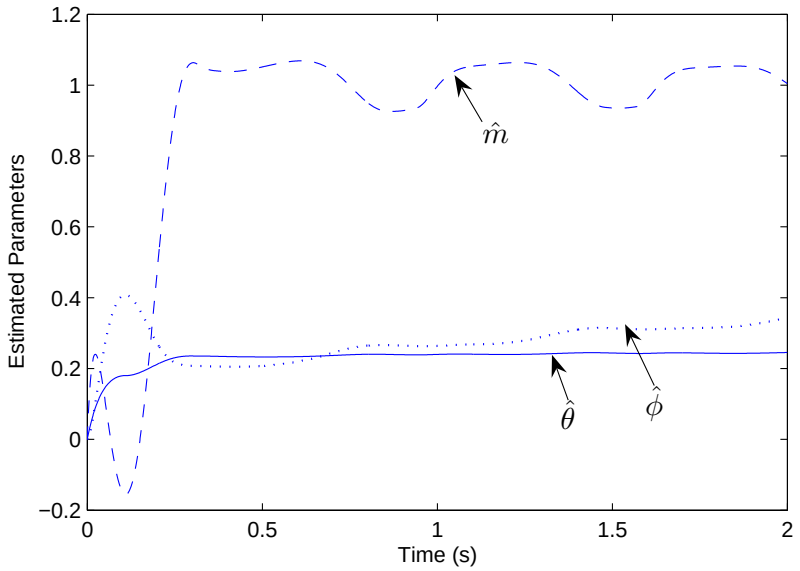

Figure 4.6: Estimated parameters trajectories

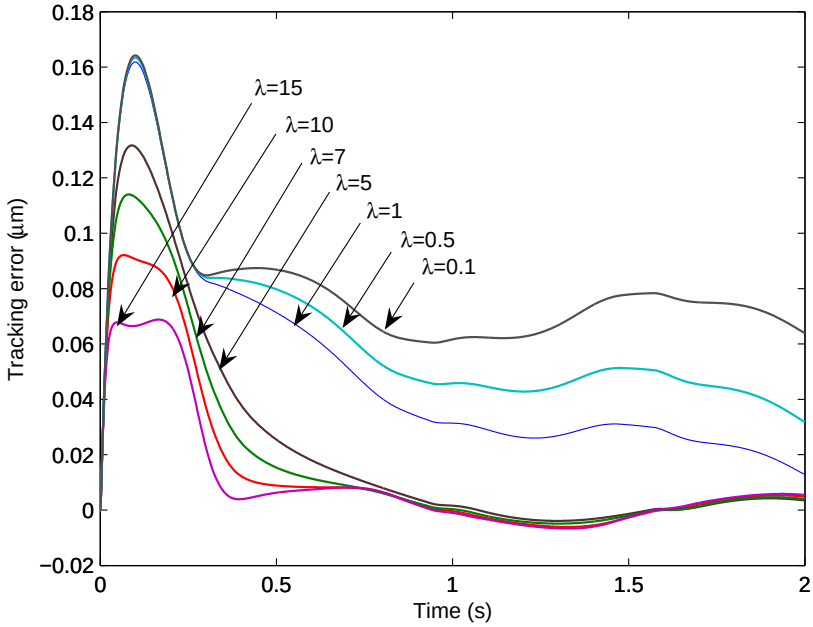

Figure 4.7: Tracking errors with different λ values

model. Using Lyapunov synthesis, adaptive neural network (NN) control algorithm was designed to achieve asymptotic tracking of the desired trajectory and guarantee the boundedness of all signals in the closed loop. Both position tracking and velocity tracking were realized at the same time by utilization of a filtered error signal. In addition, the adaptive tuning schemes was employed for the NN weights and the width of RBF functions to capture the time-varying uncertainties and nonlinearity. Simulation results show that the proposed robust adaptive NN control is effective for compensation of hysteresis friction nonlinearities and the external disturbances.

Chapter 5

Experimental Studies

5.1 Introduction

For controller assessment, experimental verification and its implementation results results are discussed, in this chapter, for tracking of sinusoidal and step demands. The proposed adaptive neural networks (NNs) controller are implemented on commercially available 3.5-inch hard disk drive (Seagate Barracuda 7200.10) with highly advanced and accurate equipments. The procedures for actual experimental platform and the development of proposed control algorithm in dSPACE real time control desk are discussed in Section 5.2. The HDD plant model in frequency domain is given in Section 5.3 with the use of persistent excitation of swept sine signal while the existence of friction is experimentally verified thorough the use of the measured frequency frequency response of VCM actuator in Section 5.4. To show the effectiveness of

proposed control algorithm, extensive implementation results are presented in Section 5.5 before the conclusion is drawn in Section 5.6.

5.2 Experiment Setup

The following key software and hardware tools are used to obtain our implementation results.

dSPACE System (DS1104) The dSPACE DSP system is used in the actual implementation throughout this thesis because of its special design for development of high-speed multivariable controllers and real-time tests. The following main components include in dSPACE sytem as described in [2]:

- Real-time Interface (RTI) and Real-time Workshop (RTW): The function of RTI is to act as a link between Simulink and the dSPace hardware. The builtin hardware control functions and blocks for DS1102 add-on card are already included in RIT. It automatically generates real-time codes from Simulink offline models and implements these codes on the dSpace real-time hard ware;

- dSPace Add-on Card: The dSpace add-on card DS1102 is essential component of dSpace DSP system and it is built on a Texas Instruments TMS320C31 floating-point DSP. As a supplement, a set of analog-to-digital (A/D) converters and digital-to-analog (D/A) converters, a DSP microcontroller based on digital I/O

subsystem and sensor interfaces are integrated to DSP system RIT and dSPace Add-on Card.

- dSpace Control desk: It is mainly used for controlling, monitoring and automating on the actual HDDs throughout experimental verifiction. It is a software platforms with a combination of dSPace Add-on Card, Simulnik and TRI workshop.

Polytec Laser Doppler Vibrometer

It is well know as an optical instrument that is used to measure vibration and displacement of vibrating surface without contact. It consists of an optical sensor head or fiber optic unit for the purpose of measuring the dynamic Doppler shift from the vibrating object. A controller or a processor is used to provide power to the optics and demodulates the Doppler information using various types of Doppler signal decoder electronics, thereby an analog velocity or displacement is produced.

In our implementation, the Polytec LDV is used to measure the displacement and velocity of the R/W heads of HDDs by directing the laser beam to the tip of R/W head and the vibration ampliture and frequency are extracted from the Doppler shift of the laser beam frequency due to the motion of R/W head. The small displacement of the actuator are captured by projecting laser beam into R/W head and convert it to an voltage output signal. The output of an LDV is generally a continuous analog voltage that is directly proportional to the target velocity component along

the direction of the laser beam. The voltage output is connected to the dSPACE control desk when the control algorithm is running during actual experiment and connected to DSA while the system model identification is carried out.

Dynamic Signal Analyzer

The Dynamic Signal Analyzer (HP35670A) is a dynamic monitoring and measuring instrument that can be used for characterizing the performance and stability of a control system. In time domain, the performance such as rise time, overshoot and settling time are generally specified while the stability criteria, gain and phase margins are generally specified in frequency domain. In our implementation, it is mainly used for model identification and obtaining the responses of the servo system in frequency domain. The two channels of DSA, CH1 (Channel 1) and CH2 (Channel 2) are used as the input and output while measuring frequency response of VCM actuator. The actual displacement of actuator tip is obtained with the aid of Laser Doppler Vibrometer (LDV) and the actuator movement is driven by voice coil motor (VCM), which is in turn powered by VCM driver.

Vibration Free Table

With the need of accurate measurement on very small displacements ($< 1/mum$), the HDD implementation set-up should be isolated from the external vibrations. Thus, the vibration free table (Vibraplane Model 9100/9200 series) is used in this implementation. Since it can provide effective isolation of vibration at frequencies

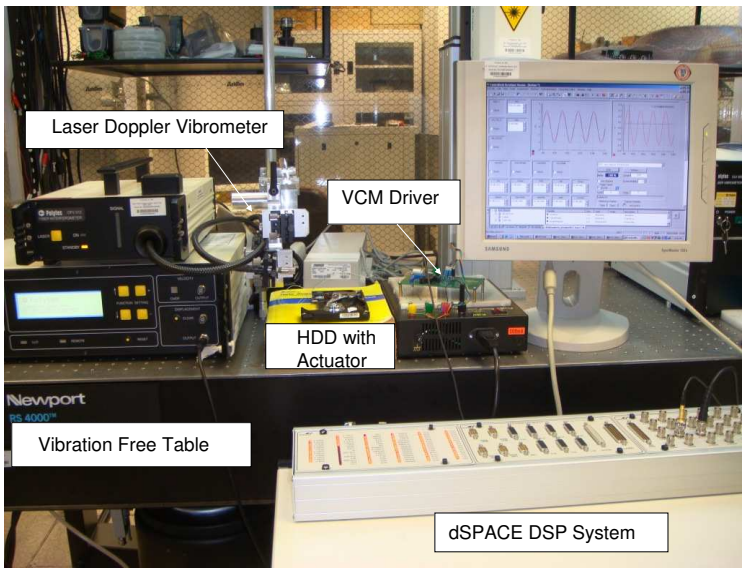

Figure 5.1: Experimental setup

above 5 Hz and low amplification at low frequency $2-3$ Hz, the improvements in resolution and repeatability of the measurement can be seen significantly in actual implementation.

To make our work more complete, the proposed control design is implemented on actual HDDs with some highly advanced and accurate equipment that are briefly summarized in Section (5.2). The actual experiments are conducted on a dSPACE, digital signal processor with a sampling time $T = 0.1ms$ as can be seen in Figure 5.1. A VCM actuator from commercial 3.5-inch hard disk drive (Seagate Barracuda 7200.10) is used for the verification of proposed adaptive NN control algorithm. The hard disk drive is partially cut off to measure the read/write head displacement of VCM actuator using the Laser-Doppler-Scanning-Vibrometer (LDV) with a resolution

set to $8\mu m/V$. The measured R/D head displacement is fed into the dSPACE digital signal processing system to generate necessary control input signals.

5.3 Frequency-domain Identification of HDD Actuator

In the experimental studies of HDD servos, the system identification is a popular method to obtain the plant modeling with persistent excitation of swept sine signal. The swept sine signal obtained from the Dynamic Signal Analyzer (DSA) is used to measure the VCM frequency response. The Laser Doppler Vibrometer (LDV) can be used to measure the movement of R/W head of HDD actuator, which allows non-contacting measurement of velocity and displacement. The schematic of our experimental set-up is shown in Figure 5.2. The excitation swept sine signal and the LDV output are fed to channel one and two of DSA and the magnitude of measured frequency response is in the unit of $\mu m/V$. To keep the actuator motion within acceptable range of LDV, the amplitude of swept sine signal is carefully chosen as 100 mV for low frequency. At higher frequency of excitation, the actuator response is attenuated and the input amplitude is chosen 50 mV - 1 V to get a better measurement of gain and phase. Since, no additional sensors/transducers are attached to actuators, the dynamics of the measured mechanical system does not change.

As investigated in [42] [60] [61], the modeling of VCM actuator in hard disk drive system could be described as the behavior of double integrator model which possess

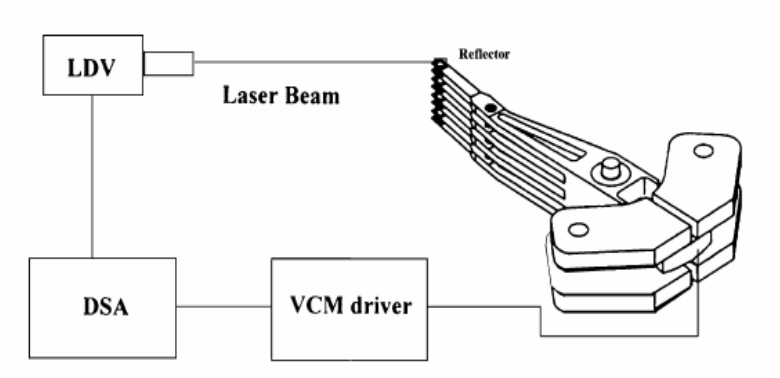

Figure 5.2: Schematic diagram for measurement of frequency response (source: [1])

-40 $db/decade$ slope in the magnitude response and $-180°$. The input-output frequency characteristic of VCM actuator with magnitude and phase response is sown in Figure 5.3. The frequency response is measured for the range of frequencies form 10 Hz to 10 kHz and shows high frequency response resonances at 5.5kHz, 6.5kHz,7.86kHz, 15kHz respectively.

The transfer function of an actuator can be derived by the use of identification algorithm as presented in Section 3.3. The measured frequency response of VCM actuator is obtained by the use of position feedback signal of VCM actuator measured from LDV to Dynamic Signal Analyzer (DSA-Hp 35670A). In this thesis, 3.5 inch hard disk drive (Seagate Barracuda 7200.10) is used for the modeling and system identification of HDDs. As can be seen in Figure 5.3, the measured frequency response via LDV and DSA and the identified result by the use of system identification algorithm are quite well matched. By curve-fitting to the measured frequency response in Figure 3,

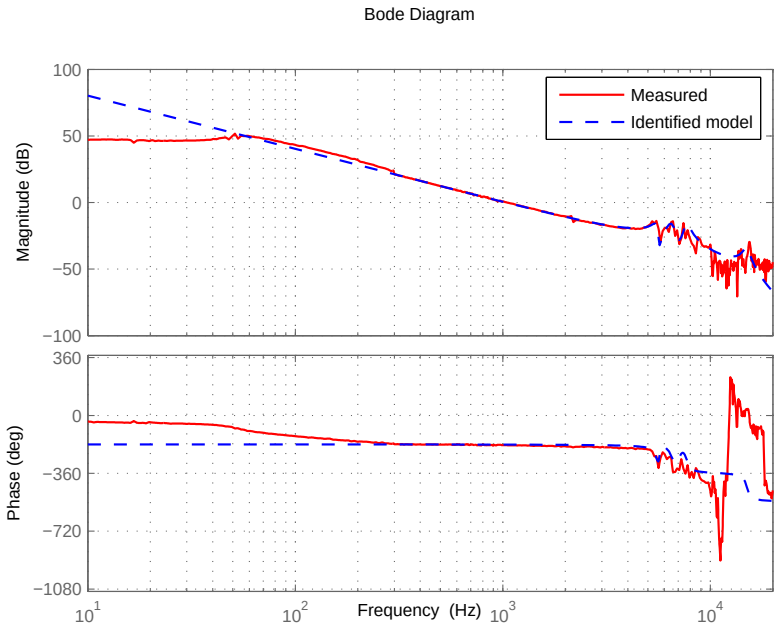

Figure 5.3: Frequency response of measured and identified HDD actuator model

we obtain the double integrator model:

$$G_P = \frac{4.0968 \times 10^7}{s^2} \tag{5.1}$$

which is independent of hysteresis friction effect; and the high frequency modes at $5.5kHz$, $6.5kHz$, $7.86kHz$, $15kHz$ are represented as follows:

$$G_{R1} = \frac{0.9321s^2 + 678.3s + 1.184 \times 10^9}{s^2 + 2053s + 1.184 \times 10^9} \tag{5.2}$$

$$G_{R2} = \frac{0.8249s^2 + 2251s + 1.665 \times 10^9}{s^2 + 3276s + 1.665 \times 10^9} \tag{5.3}$$

$$G_{R3} = \frac{2.431 \times 10^9}{s^2 + 2703s + 2.431 \times 10^9} \tag{5.4}$$

$$G_{R4} = \frac{8.383 \times 10^9}{s^2 + 5655s + 8.383 \times 10^9} \tag{5.5}$$

From Figure 5.3, it can be seen that measured frequency responses of VCM actuator and its identified frequency responses (double integrator (5.1)+ four high frequency

modes (5.2)-(5.5)) has a close match except for the low frequency range 10-200Hz, where the friction nonlinearity mainly exists.

5.4 Modeling of Pivot Friction Nonlinearity

The performance of HDD servo control loop is mainly depended on the effect of the friction of the actuator pivot. Since this problem is particularly serious in small form factor drives, much attentions on this problem have been given by mechanical engineer and control engineers. For the drives in early days, the inertia of the actuator arm was larger than that of today's actuators and the specifications for position error during track following was less stringent; such specification could be met without paying much attention to the problem of friction. To meet the demand for smaller size of drives and faster response, the inertia of the actuators has to be reduced. The effect of friction becomes noticeable with the continuous development of HDDs. The friction of the pivot produces a torque that opposes the torque generated by VCM. The friction torque is a nonlinear function which possess the position and velocity of actuator.

In [1], the frequency response of the double integrator model is expected to show $-40\ db/decade$ slope and -180° phase the the lower end of frequency. However, the experimentally obtained frequency response in Figure 5.3 shows $0db/decade$ slope and 0° phase at low frequency range 10-200Hz. In [42][61], it has been verified that

the effect of friction is manifested as reduction in gain at low frequency and the reduction depends on the amplitude of the excitation signal which is used to measure the frequency response.

It has been well known that the existence of friction can be experimentally verified thorough the use of the measured frequency frequency response of VCM actuator. If there is variation in the low frequency gain with the varying amplitude of input signal, it can be said that the friction actually exist in the practical system. As can be seen in Figure 5.4, the effect of fiction is manifested as reduction in gain at low frequency due to the amplitude variations of excitation signal that is used to measure in the frequency response. However, it is required a nonlinear model to describe the effect of nonlinear friction at low frequency region. To adopt the effect of pivot friction nonlinearity of VCM actuators obtained in Figure 5.4, several friction models have been presented in Section 2.2.

In this thesis, LuGre friction model discussed in Section 2.2.2 is adopted to represent the nonlinear behavior of the pivot friction hysteresis nonlinearity The adopted LuGre friction model introduced in (2.23) captured all the static and dynamic characteristics of hysteresis friction nonlinearity. The simulated response of LuGre friction phenomena has been presented in Figure 5.5. The curve of hysteresis friction nonlinearity can be generated by the use of the following parameters: $\sigma_0 = 10^5 \frac{N}{m}$, $\sigma_1 = \sqrt{10^5} \frac{Ns}{m}$, $\sigma_2 = 0.4 \frac{Ns}{m}$, $f_c = 1N$, $f_s = 1.5N$, $\dot{x}_s = 0.001 \frac{m}{s}$, $m = 1kg$, and the input signal $u(t) = 5sin(t)$. Different choices of parameters can result in different hysteresis

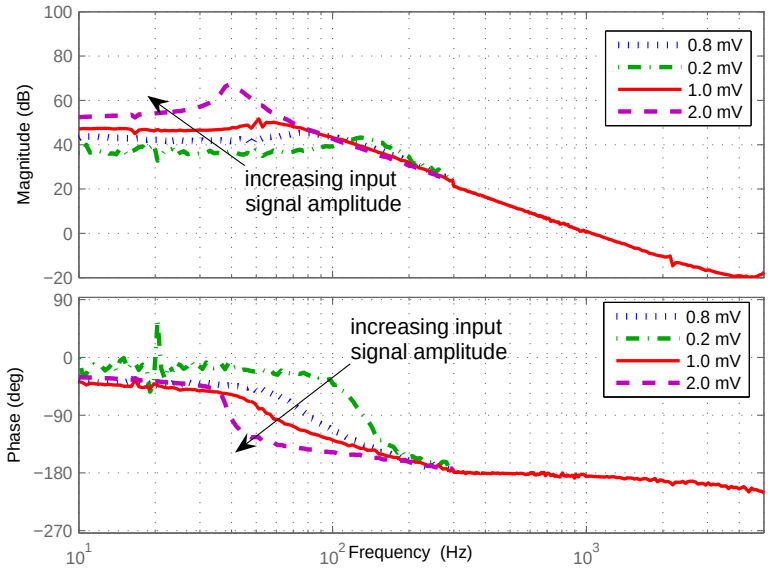

Figure 5.4: Frequency responses of VCM actuator the influence of pivot friction nonlinearity with different swept-sine input signal amplitudes at low frequency range, 10Hz-200Hz

friction nonlinearity curve shapes. Recognizing the very fact that realistic accurate hysteresis friction nonlinearity model building or parameter identification might be more difficult or complicated in practice than controller design, we adopt neural networks in control design to handle the hysteresis nonlinearity and mitigate its effect on the tracking performance.

From experimental studies, Figure 5.6 shows the hysteresis friction nonlinearity curve at low frequency 80Hz. It is consistent with the hysteresis friction curve generated by the LuGre friction model (4.2)-(4.4) in Figure 5.5. Instead of conducting parameter identifications for the LuGre friction model, we adopt neural networks to approximate

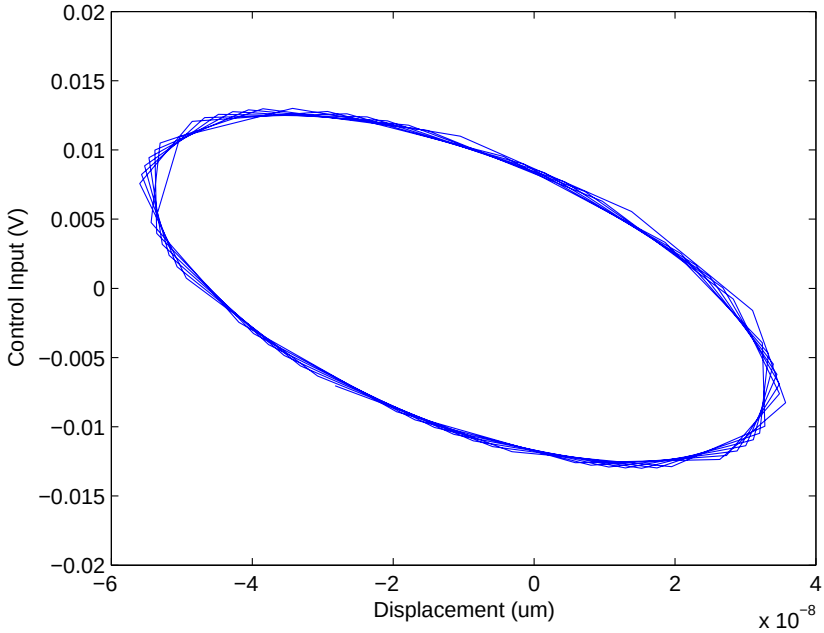

Figure 5.5: Stimulated hysteresis friction curves given by LuGre friction model in (4.1)-(4.4).

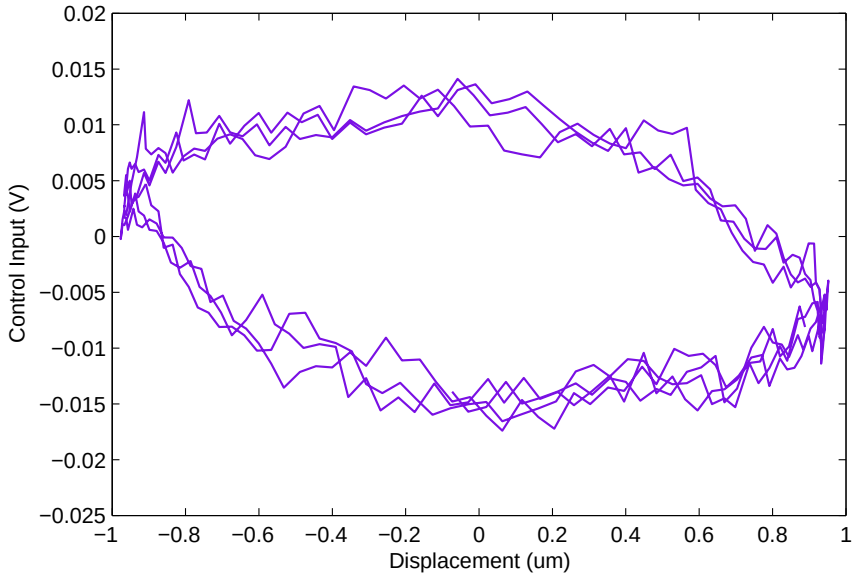

Figure 5.6: Experimental pivot hysteresis friction nonlinearity curve at frequency 80Hz

the unknown bounding function of the LuGre friction model as presented in 4.14.

5.5 Experimental Results

In this section, extensive experimental results are presented to demonstrate the effectiveness of proposed adaptive neural network (NN) control scheme for cancelation of pivot hysteresis friction nonlinearity by the use of both sinusoidal and step reference input. In Figure 5.4, it has been experimentally verified that the friction nonlinearity exist at low frequency region $10 - 200$ Hz while the existence of resonances effect at high frequency region is shown in Figure 5.3. In [62] and [63], it has been proposed that those high frequency resonances can be completely canceled by the use of notch notch filters. However, the cancelation of those high frequency resonances will not be considered in this thesis. In this thesis, our main focus is not on the high frequency resonances, but we are mainly considered the compensation of the friction nonlinearity at low frequency components. Since friction nonlinearity at the low frequency range 10-200Hz are mainly considered in this thesis, the effectiveness of proposed adaptive NN compensation schemes can be distinctly seen through out the following implementation results.

Firstly, we consider the reference signal, x_d as a sinusoidal, $x_d = A\sin(\pi f t)$, where A is the amplitude and f is the frequency. The control parameters for (4.16) and adaption laws (4.18)-(4.21) are chosen as: $\lambda = 595, k = 7.9 \times 10^{-15}, k_\theta = -1 \times 10^{-9}, k_\phi = 1.5 \times$

$10^{-6}, k_m = -2 \times 10^{-14}, k_w = 3 \times 10^{-8}, \sigma_\theta = 15 \times 10^6, \sigma_\phi = 12 \times 10^6, \sigma_m = 4.99 \times 10^{13}$, $\Gamma = diag\{1.0\}$, $\sigma_w = 7 \times 10^3$. All the initial values are set to zero. The radial basis function neural network (RBFNN) with Gaussian basis function, $\hat{W}^T S(x, \dot{x})$, has been employed with position input signal, x and velocity input signal, $\dot{x}$.

Figures 5.8 and 5.7 show that our proposed adaptive NN controller that is so called proposed friction compensator can successfully reduce the tracking error to neighborhood of zero for the sinusoidal reference signal with amplitude of $2\mu m$ and frequencies at 100 Hz. As can be seen in Figure 5.4, the friction nonlinearity exist at low frequency until 200 Hz, the proposed friction compensator is continuously studied for the sinusoidal reference signal with amplitude of $2\mu m$ and frequencies at 200 Hz. In 5.10 and 5.9, the proposed adaptive NN controller guaranteed the position error signal converged to a neighborhood of zero.

The boundedness of the parameter estimates in the proposed adaptive neural network control are presented in Figures 5.11 and 5.12. The design parameters of the proposed controller are adjusted during experimental verification. From Figure 5.20, we can see that the tracking error could be decreased by increasing the value of λ, but that increases would also increase the control signal as presented in (4.10) - (4.16), and could excite unmodeled dynamics. Therefore, caution must be exercised in the choice of these parameters, due to the fact that there are some tradeoffs between the control performance and other issues.

Secondly, the step response is investigated by choosing square wave signal as the desired trajectory. Good tracking performances for a demand step of $0.5\mu m$ and $5\mu m$ are achieved as shown in Figures 5.13, 5.14, 5.16 and 5.15. Compared with the conventional PID control, the proposed adaptive NN control can decrease the overshoot and reduce the settling time performance without degrading the tracking accuracy. Figures 5.17 and 5.18 show the boundedness of the parameter estimates. Similar to the sinusoidal case, from Figure 5.19, we can see that with the increase of λ, the convergence rate become faster, but with the price of higher overshoot. Therefore, there are also some tradeoffs in the choice of these parameters. In addition, to indicate the effect of hysteresis friction can be mitigated by NN approximation, we showed comparison studies of the hysteresis friction curve with and without NN compensation in Figure 5.21.

5.6 Conclusion

An alternative approach to pivot nonlinearity friction compensation by the use of adaptive neural network control is presented in this thesis.Through experiment results using a 3.5-in disk drive, it has been shown that the proposed friction compensator is indeed effective and guaranteed that the position error signal converged to a neighborhood of zero. Furthermore, by using a sequence of square waves as a reference, the overshooting in the time responses can be compared between servo controls with

and without compensators for friction. we have shown that the proposed adaptive NN based friction compensator is working well in practice.

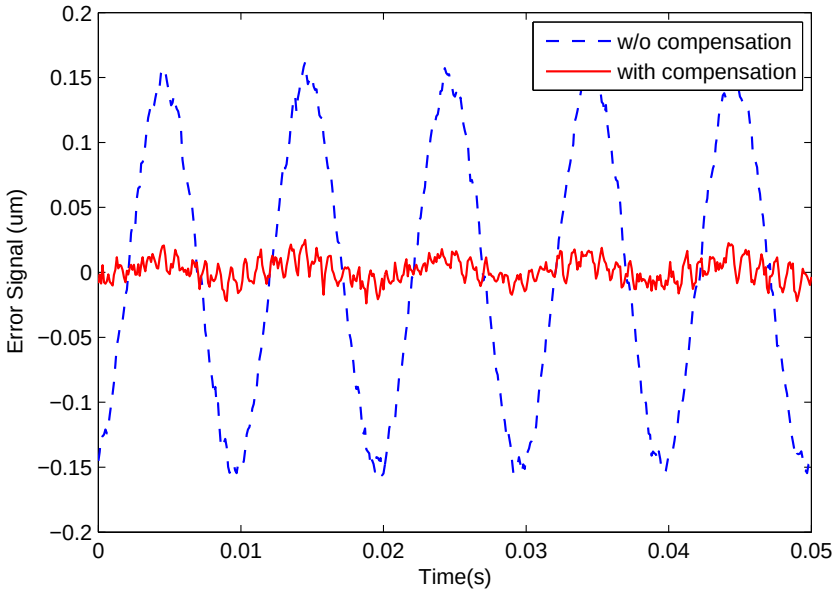

Figure 5.7: Tracking error for the desired sinusoidal trajectory with A = 2 and f = 100 Hz

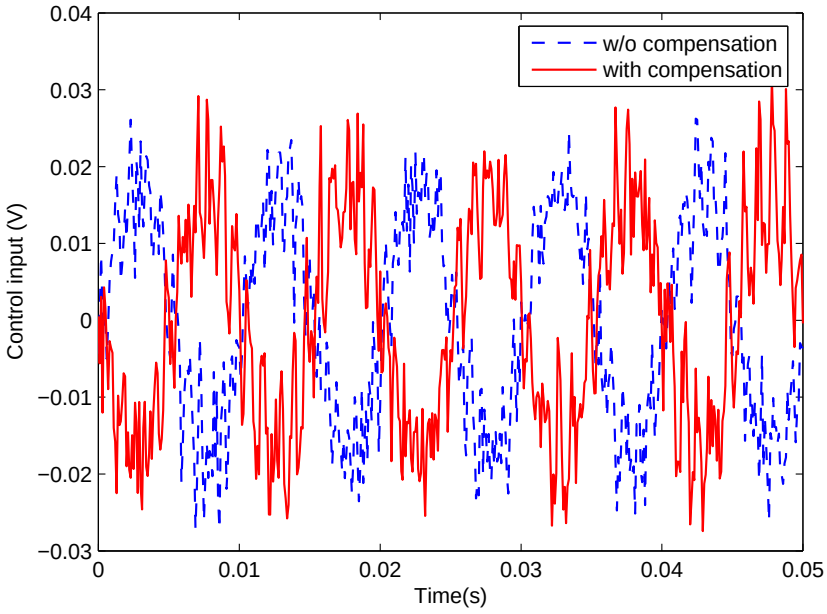

Figure 5.8: Control input signal for the desired sinusoidal trajectory with A = 2 and f = 100 Hz

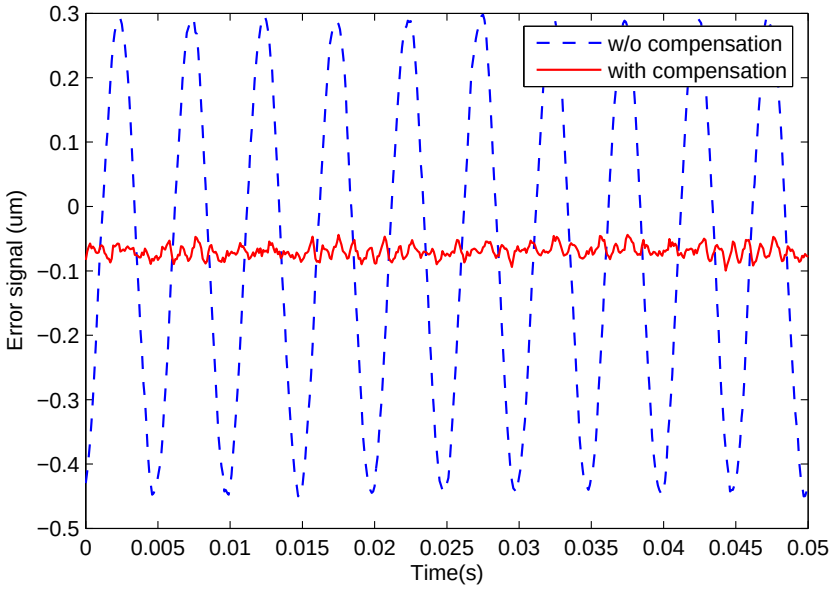

Figure 5.9: Tracking error for the desired sinusoidal trajectory with A = 2 and f = 200 Hz

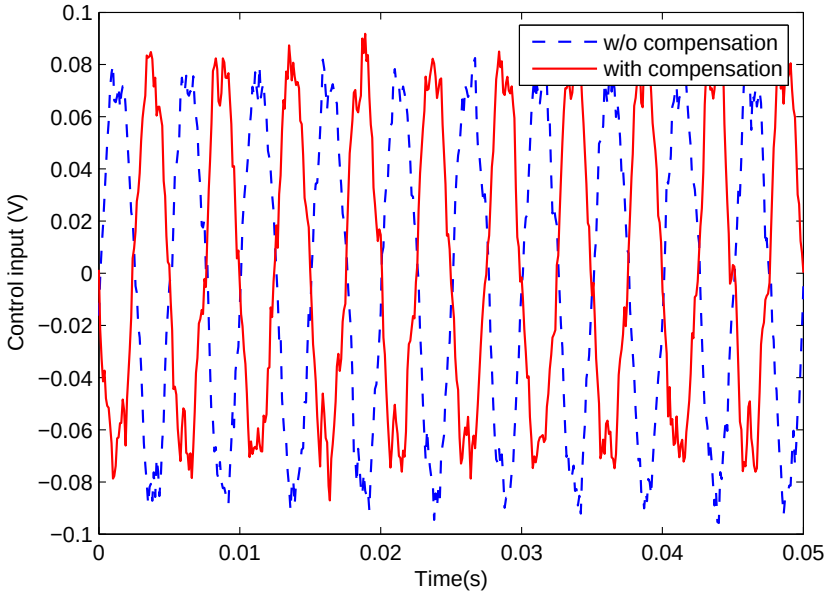

Figure 5.10: Control input signals for the desired sinusoidal trajectory with A = 2 and f = 200 Hz

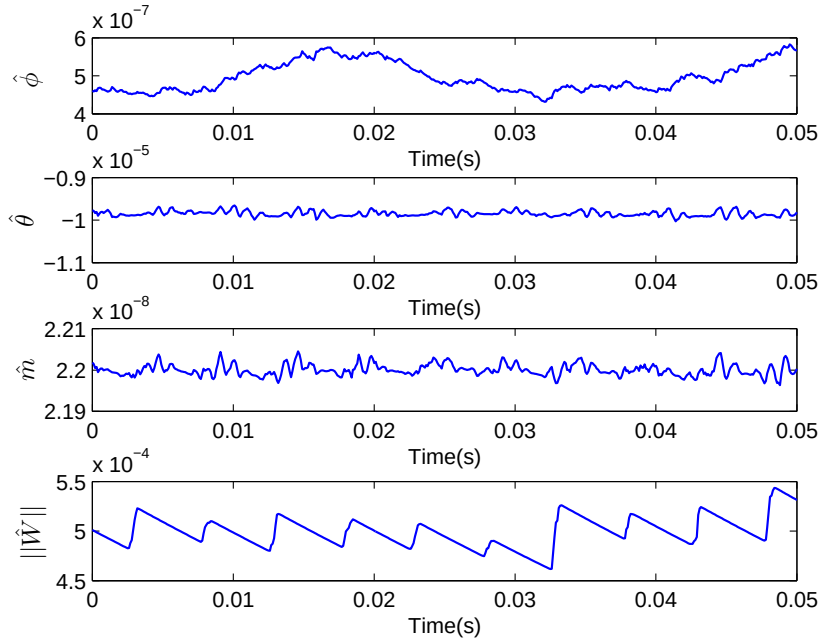

Figure 5.11: Parameters adaptations for the desired sinusoidal trajectory with A = 2 and f = 100 Hz

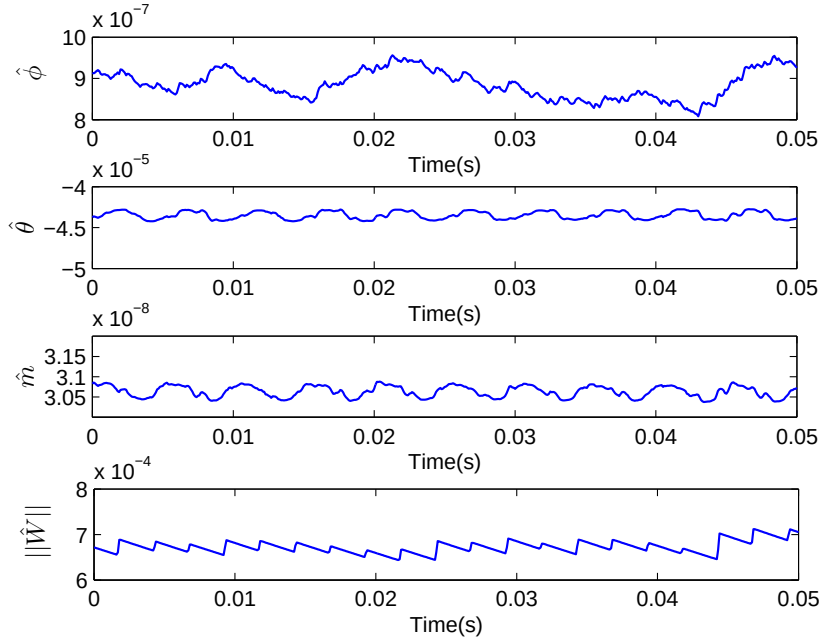

Figure 5.12: Parameters adaptations for the desired sinusoidal trajectory with A = 2 and f = 200 Hz

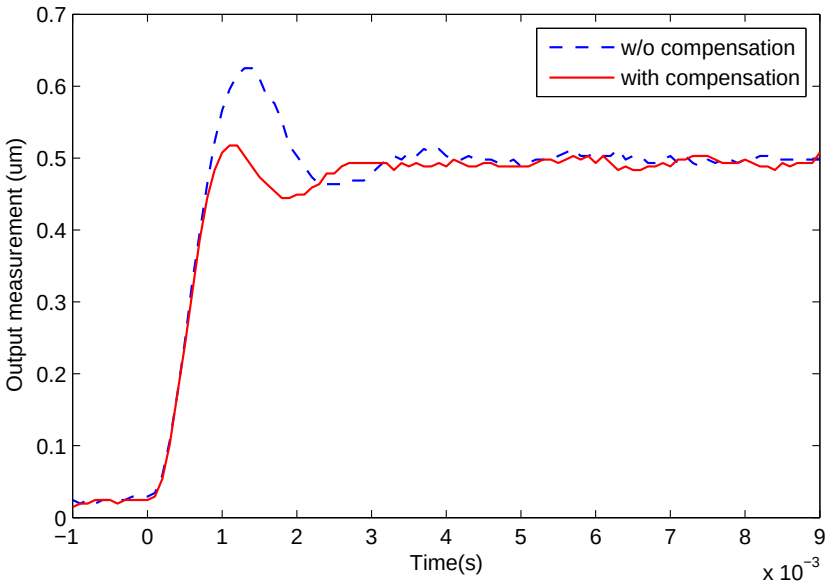

Figure 5.13: Step response with amplitude 0.5 μm

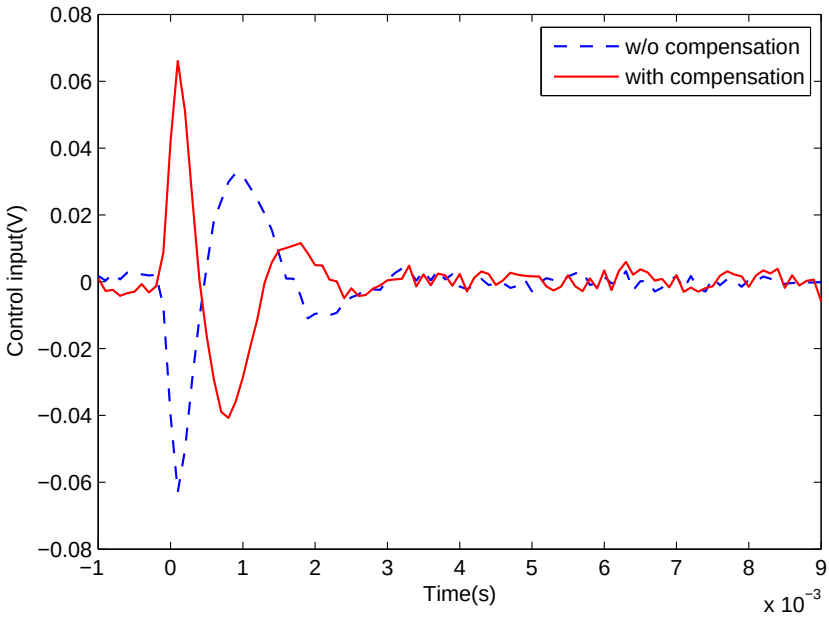

Figure 5.14: Control input signls for step response with amplitude 0.5 μm

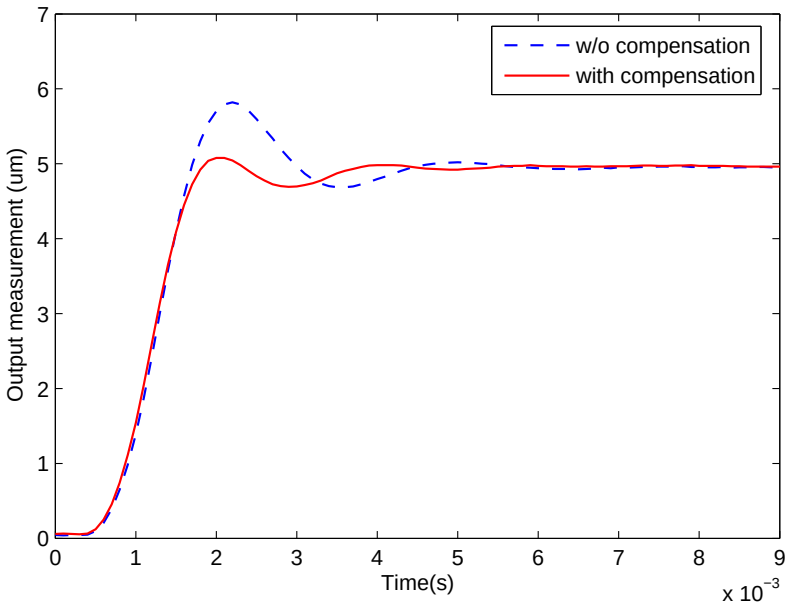

Figure 5.15: Step response with amplitude 5 μm

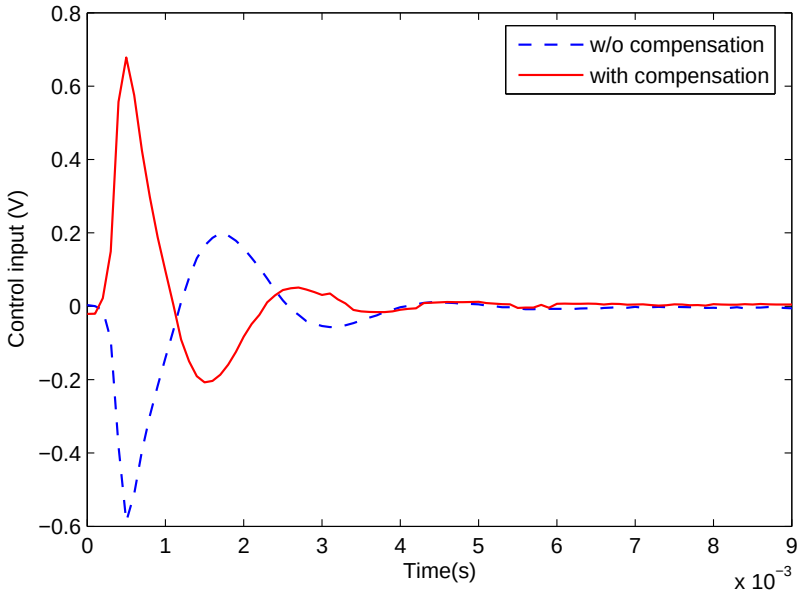

Figure 5.16: Control input signal for step response with amplitude 5 μm

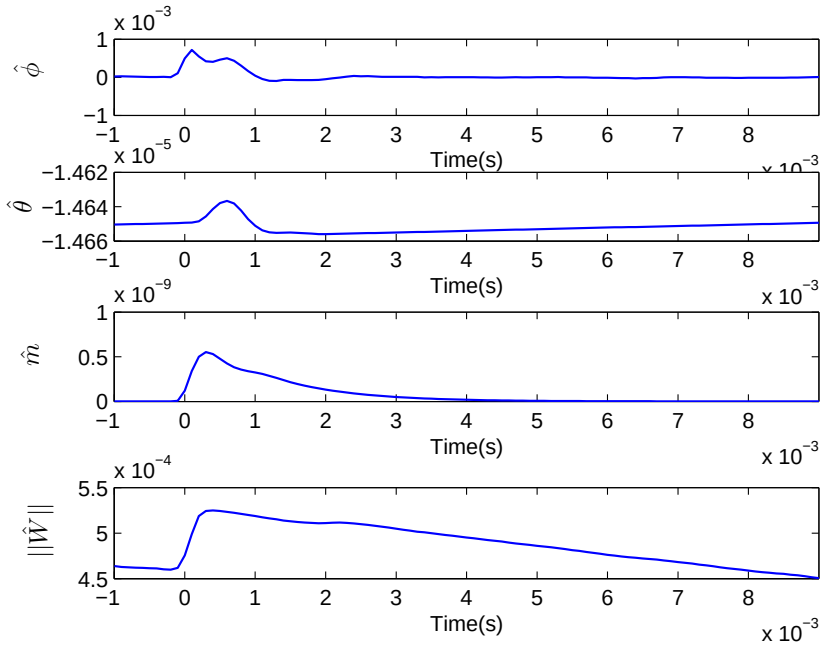

Figure 5.17: Parameters adaptations for step response with amplitude 0.5 μm

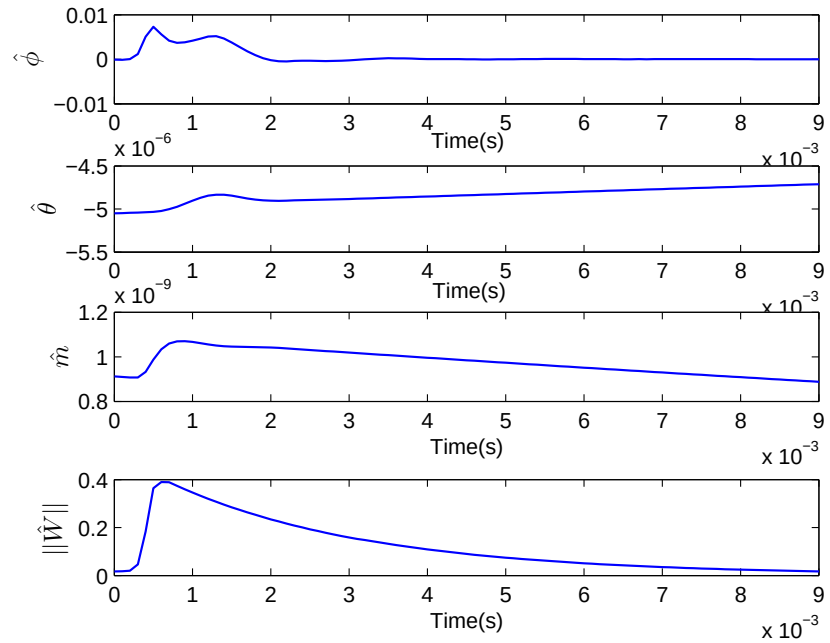

Figure 5.18: Parameters adaptations for step response with amplitude 5 μm

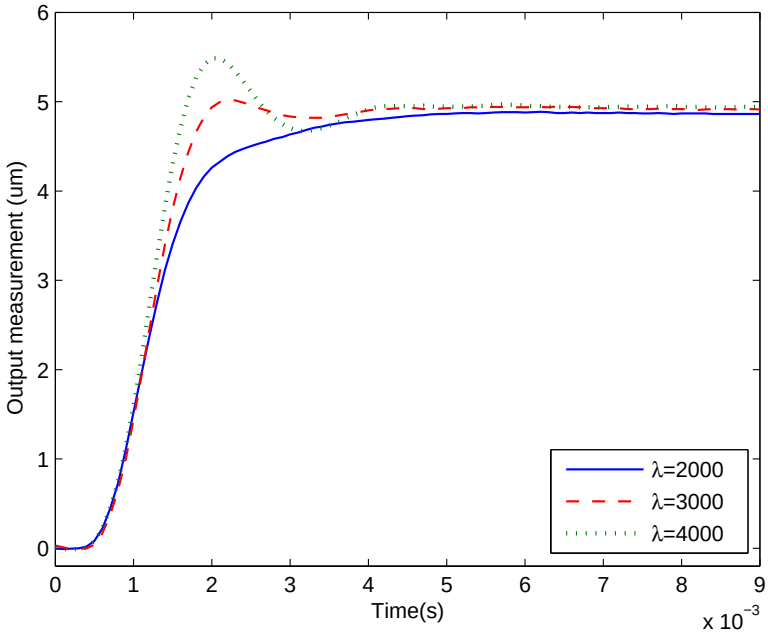

Figure 5.19: Tracking error signals with different design parameter λ for the step response with amplitude 5 μm

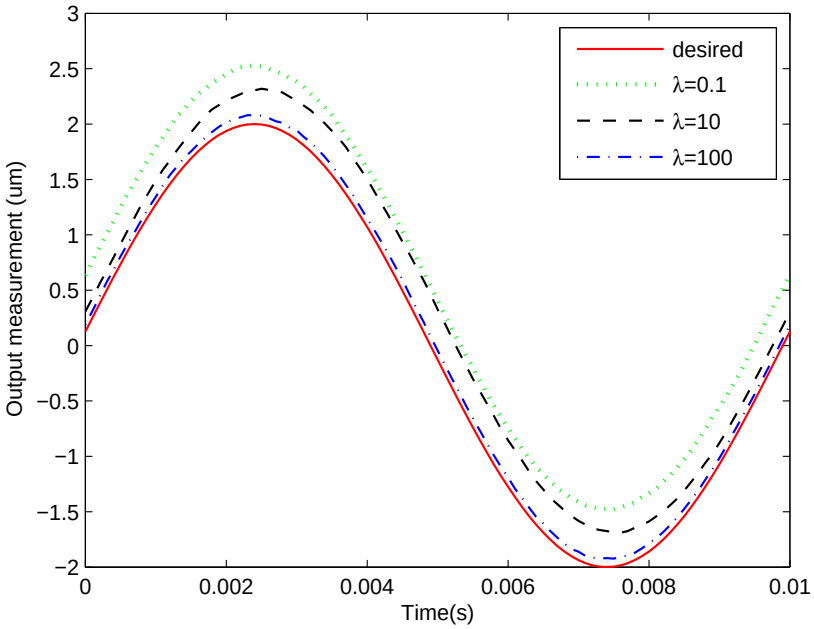

Figure 5.20: Tracking error signals with different design parameter λ for the sinusoidal respond with amplitude 2 μm

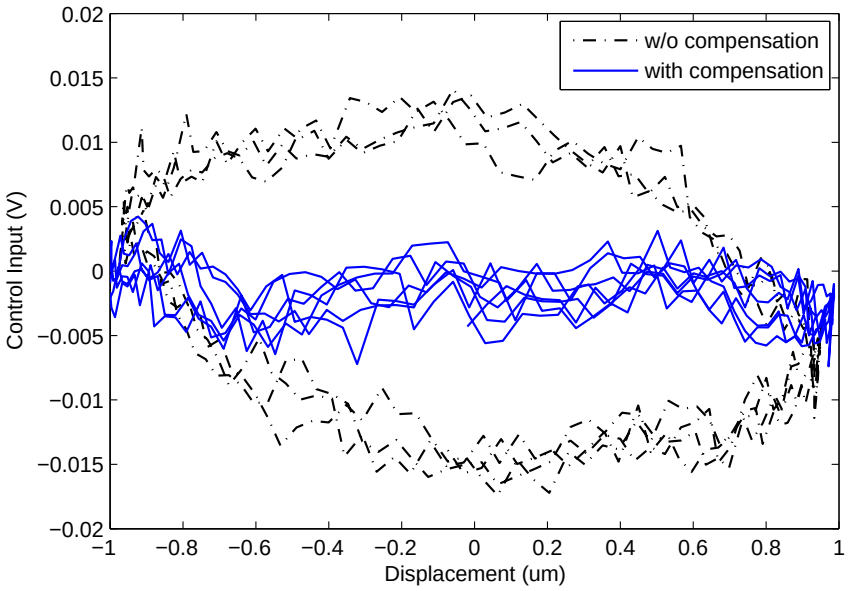

Figure 5.21: Comparison results of experimental pivot hysteresis friction nonlinearity curves with and without friction compensation at frequency 80Hz

Chapter 6

Conclusion and Suggestion of Further Research

6.1 Conclusions

In the present research presented in previous chapters, it is more concern with the system identification and the application of adaptive neural network (NN) controller to the actual hard disk drive system. The main findings of this research work are concluded as follows:

- The first part of thesis, Chapter 1, is covering with some background introduces to HDD servo systems and components of HDDs are discussed in detail. The servo system and servo control challenges by servo engineers and researchers

are also discussed. The rigorous analysis on the various sources of disturbances, nonlinearities and uncertainties of a typical hard disk drive servo system are presented before the objectives, scopes and organization of thesis are given.

- The comprehensive studies of nonlinear phenomenons and its compensation methodologies which have been widely used in cancelation of friction and other nonlinearities of HDDs are presented in Chapter2. To adopt the effect of pivot friction nonlinearity of VCM actuators, several friction model are discussed in Section 2.2. Additionally, the choice of nonlinear friction friction model through the use of frequency domain identification algorithm is aslo given Section in 2.3.

- Chapter 3 dealt with some commonly used system identification and modeling techniques which are used in both time and frequency domain are presented. The mathematical model of the VCM actuator in time domain are given in Section 3.2 while frequency domain identification algorithm for obtaining transfer function model are presented in Section 3.3.

- Chapter 4 focus on the design of an improved adaptive neural network (NN) controller for compensation of pivot friction hysteresis nonlinearity. To achieve asymptotic tracking of the desired trajectory and guarantee the boundedness of all signals in the closed loop, an adaptive neural network (NN) control algorithm was developed in Section 4.2.1 by the use of Lyapunov synthesis. In addition, the adaptive tuning schemes was employed for the NN weights and the width

of RBF functions to capture the time-varying uncertainties and nonlinearity.

- The procedures for actual experimental platform and the development of proposed control algorithm in dSPACE real time control desk are discussed in Section. 5. The identification of HDD plant model in frequency domain and its obtained transfer function model are also presented in 5.3. The existence of friction is experimentally verified thorough the use of the measured frequency frequency response of VCM actuator in Section 5.4 while the extensive implementation results are presented in Section 5.5.

6.2 Recommendations for Further Research

It is possible to make improvement to the ideas and techniques contained in this thesis as well as extend to other applications.

This thesis has been emphasized on comprehensive features of friction nonlinearity for typical VCM actuator used in hard disk drive system. The detailed analysis has been carried out on pivot bearing hysteresis nonlinearity by the use of LuGre friction model which capture all the static and dynamic characteristics of hysteresis friction nonlinearity. The verification of the adopted hysteresis model shows it indeed describes the features the friction nonlinearity of VCM actuator. By considering the position and velocity tracking control of a servo mechanism with hysteresis friction, an adaptive NN friction compensation scheme was developed in this thesis. Extensive

implementation results are also discussed to demonstrate the effectiveness of proposed adaptive neural network (NN) control scheme for cancelation of pivot hysteresis friction nonlinearity by the use of both sinusoidal and step reference input. In addition, it can also shows that the effect of the hysteresis friction can be mitigated well by NN approximation thorough out the comparison studies of with and without NN compensation scheme.

Besides the above friction compensation for hard disk drive servomechanism, there are many factors which are simplified or neglected in this thesis. With the increase of storage capacity and data transfer rate for high performance servo system, it is necessary to achieve more precise positioning of the R/W head during track seeking or track following performance. In order to improve the servo performance of HDDs, improved intelligent control methodologies are still crucial. It will be better if the following factors taken into consideration for HDD servomechanism.

- **Intelligent feedforward: adaptive neural network compensation of disturbances compensation:**

  In recent years, the data density on magnetic disk drives has increased significantly corresponding to a decrease in data track width and thus allowable position error of the read/write (R/W) heads. The demand for better tracking performance of the VCM actuator faces challenges subject to external vibrations and shocks as they are increasingly used in mobile applications. To reduce the

effect of disturbances on the hard disk drives, several methods have been proposed using accelerometers to measure external disturbances and injecting the accelerometer signal to a feedforward controller. However, the mathematical models of the disturbance dynamics must be know or partly known to use those mentioned feedforward controller. Because of the distinct advantages of neural networks as nonlinear controllers over conventional controllers in achieving desired performances, they have received considerable attention in the control community. The efficacy of neural network feedforward compensator in rejecting the effect of disturbances, an adaptive feedforward compensator is suggested as a further improvement of this thesis.

- **Adaptive resonance compensation:**

  In hard disk drives (HDD) servo systems, mechanical resonance exist from Voice Coil Motor (VCM) actuator structure in the form of vibrations. It can lead to performance degradation or even instability of hard disk drive servo system if not properly handled by the design of servo controller. To suppress these resonance modes, diverse resonance cancelation methodologies have been proposed in many literatures. Notch filters are generally used to cancel these mechanical resonance modes. In addition, adaptation algorithms for notch filters have been developed to compensate those resonances. Besides adaptive notch filters, indirect adaptive compensation (IAC), and structurally parallel compensation (SPC) were also proposed for resonant mode compensation in HDD dual stage

actuation systems. To get perfect servo control of hard disk drive systems, I would like to suggest to design direct robust adaptive compensator for attenuation of uncertain resonance dynamics based on the previous works on adaptive control of servo mechanisms and intelligent control of HDDs.

Bibliography

[1] A. A. Mamun, G. Guo, and C. Bi, *Hard disk drive mechatronics and control*. New York: CRC Press, 2007.

[2] K. B.M.Chen, T.H.Lee and V. Venkataramanan, *Hard Disk Drive Servo Systems*. New York: Springer, 2006.

[3] J. W. Macki, P. Nistri, and P. Zecca, "Mathematical models for hysteresis," *SIAM Review*, vol. 35, no. 1, pp. 94–123, 1993.

[4] F. Hong and C. Du, "An improved adaptive neural network compensation of pivot nonlinearity in hard disk drives," *IEEE International Workshop on Advanced Motion Control*, vol. 12, no. 6, pp. 440 – 443, 2008.

[5] R. W. Wood, J. Miles, and T. Olson, "Recording technologies for terabit per square inch systems," *IEEE Transactions on Magnetics*, vol. 38, no. 4, pp. 1711–1718, 2002.

[6] B. Knigge, O. Ruiz, and P. Baumgart, "Minimum stable flying height with thermal protrusion actuation," *Asia-Pacific Magnetic Recording Conference*, pp. 1 – 2, 2006.

[7] L. Xinqun, D.Jenkins, and P. Davey, "Head disk spacing variation suppression via active flying heightcontrol," *Proceedings of the 18th IEEE Instrumentation and Measurement Technology Conference*, vol. 2, pp. 888 – 891, 2001.

[8] J. Y. Juang, D. Chen, and D. B. Bogy, "Alternate air bearing slider designs for areal density of 1 tb/in2," *IEEE Transactions on Magnetics*, vol. 42, no. 2, pp. 145 – 150, 2005.

[9] B. Liu, C. H. Wong, and W. Hua, "Low flying-height slider with high thermal actuation efficiency and small flying-height modulation caused by disk waviness," *IEEE Transactions on Magnetics*, vol. 44, no. 1, pp. 145 – 150, 2008.

[10] T. R. Albrecht and F. Sai, "Load/unload technology for disk drives," *IEEE Transactions on Magnetics*, vol. 35, no. 2, pp. 857–862, 1999.

[11] C. D. Mee and E. Daniel, *Magnetic recording.* New York: McGraw-Hill, 1987.

[12] V. Venkataramanan, B. M. Chen, T. H. Lee, and G. Guo, "Improvement of servo performance via nonlinear feedback control in hard disk drive servo systems," *Proceedings of the 39th IEEE Conference on Decision and Control*, vol. 4, no. 0, pp. 3088–3093, 2000.

[13] C. D. Mee and E. Daniel, *Magnetic recording technology.* New York: McGraw-Hill, 1996.

[14] Q. Li, O. E. Hong, and M. A. Manna, "The analysis of the dynamics of 3.5 inches hard disk drive actuators," *Technical Reprot: Data Storage Institute*, 1997.

[15] D. Y. Abramovitch, "Rejecting rotational disturbances on small disk drives using rotational accelerometers," *Proceedings of the IFAC World Congress*, pp. 1–6, 1996.

[16] S. E. Baek and S. H. Lee, "Vibration rejection control for disk drives by accelerationfeedforward control," *Proceedings of the 38th IEEE Conference on Decision and Control*, vol. 5, pp. 5259–5262, 1999.

[17] C. L. Du, S. S. Ge, and F. Lewis, "H-infinity compensation of external vibration impace on servo performance of hard disk drives in mobile applications," *International Journal of Adaptive Control and Signal Processing*, vol. 22, pp. 374–387, 2008.

[18] S. Pannu and R. Horowitz, "Adaptive accelerometer feedforward servo for disk drives," *Proceedings of the 36th IEEE Conference on Decision and Control*, vol. 5, pp. 4216–4218, 1997.

[19] A. Jinzenji, T. Sasamoto, and K. Aikawa, "Acceleration feedforward control against rotational disturbance in hard disk drives," *IEEE Transactions on Magnetics*, vol. 37, no. 2, pp. 888–893, 2001.

[20] K. Usui, M. Kisaka, A. Okuyama, and M.Nagashima, "Reduction of external vibration in hard disk drives using adaptive feed-forward control with single shock sensor," *9th IEEE International Workshop on Advanced Motion Control*, pp. 138–143, 2006.

[21] M. T. White and M. Tomizuka, "Increased disturbance rejection in magnetic disk drives by acceleration feedforward control and parameter adaptation," *Control Engineering Practice*, vol. 5, no. 6, pp. 741–751, 1997.

[22] S. S. Ge and C. Wang, "Adaptive neural control of uncertain mimo nonlinear systems," *IEEE Transactions on Neural Networks*, vol. 15, no. 3, pp. 741–751, 2004.

[23] E. B. Kosmatopoulos, M. M. Polycarpou, M. A. Christodoulou, and P. A. Ioannou, "High-order neural network structures for identification ofdynamical systems," *IEEE Transactions on Neural Networks*, vol. 6, no. 2, pp. 422–431, 1995.

[24] F. L. Lewis, A. Yesildirek, and K. Liu, "High-order neural network structures for identification ofdynamical systems," *Proceedings of the 32nd IEEE Conference on Decision and Control*, vol. 3, pp. 2785–2791, 1993.

[25] F. L. Lewis, S. Jagannathan, and M. J. Mears, *Neural network control of robot manipulators and nonlinear systems.* London: Taylor and Francis, 1999.

[26] M. M. Polycarpou and M. J. Mears, "Stable adaptive tracking of uncertain systems using nonlinearly parametrized on-line approximators," *International Journal of Control*, vol. 70, no. 3, pp. 363–384, 1998.

[27] C. L. Lin and Y. H. Hsiao, "Adaptive feedforward control for disturbance torque rejection inseeker stabilizing loop," *IEEE Transactions on Control Systems Technology*, vol. 9, no. 1, pp. 108–121, 2001.

[28] D. Gorinevsky and L. A. Feldkamp, "Rbf network feedforward compensation of load disturbance in idlespeed control," *IEEE Control Systems Magazine*, vol. 16, no. 6, pp. 18–27, 1996.

[29] P. A. Weaver and R. M. Ehrlich, "The use of multirate notch filters in embedded-servo disk drives," *Proceedings of the American Control Conference*, vol. 6, pp. 4156–4160, 1995.

[30] D. P. Magee, "Optimal filtering to improve performance in hard disk drives:simulation results," *Proceedings of the American Control Conference*, vol. 1, pp. 71–75, 1999.

[31] C. I. Kang and C. H. Kim, "An adaptive notch filter for suppressing mechanical resonance in high track density disk drives," *Microsystem Technologies*, vol. 11, no. 8, pp. 638–652, 2005.

[32] G. G. D. Wu and T. C. Chong, "Comparative analysis on resonance compensation in hdd dual-stage actuation systems," *IEEE Transactions on Industrial Electronics*, vol. 50, no. 6, pp. 1179– 1186, 2003.

[33] B. Armstrong-Hlouvry, P. Dupont, and C. C. D. Wit, "A survey of models, analysis tools and compensation methods for the control of machines with friction," *Automatica*, vol. 30, no. 7, pp. 1083–1138, 1994.

[34] X. Liu and J. C. Liu, "Analysis and measurement of torque hysteresis of pivot bearing in hard disk drive applications," *Tribology International*, vol. 32, pp. 125–130, 1999.

[35] D. Abramovitch, F. Wang, and G. Franklin, "Disk drive pivot nonlinearity modeling part I: frequency domain," in *Proceedings of the American Control Conference*, (Baltimore, Maryland), pp. 2600–2603, 1994.

[36] F. Wang, T. Hurst, D. Abramovitch, and G. Franklin, "Disk drive pivot nonlinearity modeling part II: Time domain," in *Proceedings of the American Control Conference*, (Baltimore, Maryland), pp. 2604–2607, 1994.

[37] H. T. Goh, S. Weerasooriya, T. S. Low, and Y. H. Huang, "Modeling and compensation of pivot friction in a disk drive actuator," in *Proceedings of the American Control Conference*, (Seattle, Washington), pp. 4141–4145, 1995.

[38] D. Karnopp, "Computer simulation of stick-slip friction in mechanical dynamic systems," *Journal of Dynamic Systems, Measurement, and Control*, vol. 107, no. 1, pp. 100–103, 1985.

[39] J. Q. Gong, L. Guo, H. S. Lee, and B. Yao, "Modeling and cancellation of pivot nonlinearity in hard disk drives," *IEEE Transactions on Magnetics*, vol. 38, no. 5, pp. 3560–3565, 2002.

[40] K. Peng, B. M. Chen, G. Cheng, and T. H. Lee, "Modeling and compensation of nonlinearities and friction in a micro hard disk drive servo system with nonlinear feedback control," *IEEE Transactions on Control Systems Technology*, vol. 13, no. 5, pp. 708–721, 2005.

[41] J. Ishikawa and M. Tomizuka, "Pivot friction compensation using an accelerometer and a disturbance observer for hard disk drives," *IEEE/ASME Transactions on Mechatronics*, vol. 3, no. 3, pp. 194–201, 1998.

[42] T. Yan and R. Lin, "Experimental modeling and compensation of pivot nonlinearity in hard disk drives," *IEEE Transactions on Magnetics*, vol. 39, no. 2, pp. 1064–1069, 2003.

[43] T. Huang, Y. Ding, S. Weerasooriya, and T. S. Low, "Disk drive pivot nonlinearity modeling and compensation through fuzzy logic," *IEEE Transactions on Magnetics*, vol. 34, no. 1, pp. 30–35, 1998.

[44] S. S. Ge, T. H. Lee, and S. X. Ren, "Adaptive friction compensation of servo mechanisms," *International Journal of Systems Science*, vol. 32, no. 4, pp. 523–532, 2001.

[45] G. Herrmann, S. S. Ge, and G. Guo, "Practical implementation of a neural network controller in a hard disk drive," *IEEE Transactions on Control Systems Technology*, vol. 13, no. 1, pp. 146–154, 2005.

[46] C. C. de Wit, H. Olsson, K. J. Astrom, and P. Lischinsky, "A new model for control of systems with friction," *IEEE Transactions on Automatic Control*, vol. 40, no. 3, pp. 419–425, 1995.

[47] B. Armstrong-Helouvry, P. Dupont, and C. C. de Wit, "A survey of analysis tools and compensation methods for the control of machines with friction," *Automatica*, vol. 30, no. 7, pp. 1083–1138, 1994.

[48] B. Armstrong, "Stick-slip arising from stribeck friction," in *IEEE Int. Conf. Robotics and Automation*, pp. 1377–1382, 1990.

[49] A. Tustin, "The effects of backlash and of speed-dependent friction on the stability of closed-cycle control system," *Journal Institution of Electrical Engineers*, vol. 94, no. 2, pp. 143–151, 1947.

[50] B. Armstrong, "Friction experimental determination, modeling and compensation," in *IEEE Int. Conf. Robotics and Automation*, pp. 1422–1427, 1988.

[51] C. C. de Wit, C. P. Noel, A. Auban, and B. Brogliato, "Adaptive friction compensation in robot manipulators: low velocities," *Intnational Journal of Robotics Research*, vol. 10, no. 3, pp. 189–199, 1991.

[52] D. P. Hess and A. Soom, "Friction at a lubricatal line contact operating at oscillating sliding velocity," *Journal of Tribology*, vol. 112, no. 1, pp. 147–152, 1990.

[53] P. Dahl, "A solid friction model," *The Technical Report TOR-0158H310718I-1*, vol. Aerospace Corporation, pp. El Segundo, CA, 1968.

[54] P.-A. Bliman, "Mathematical study of the dahls friction model," *European Journal of Mechanics. A/Solids*, vol. 11H6I, p. 835848, 1992.

[55] C. C. de Wit, H. Olsson, K. J. Astrom, and P. Lischinsky, "A new model for control of systems with friction," *IEEE Transactions on Automatic control*, vol. 40, no. 3, pp. 419–425, 1995.

[56] P. Eykhoff, *System identification - paramter and state estimation*. New Jersey: John Wiley

[57] R. M. Sanner and J. E. Slotine, "Gaussian networks for direct adaptive control," *IEEE Transactions on Neural Networks*, vol. 3, no. 6, pp. 837–863, 1992.

[58] S. S. Ge, C. C. Hang, T. H. Lee, and T. Zhang, *Stable Adaptive Neural Network Control*. Boston: Kluwer Academic Publisher, 2002.

[59] B. B. Ren, P. P. San, S. S. Ge, and T. H. Lee, "Robust adaptive nn control of hard disk drives with hysteresis friction nonlinearity," *Proceedings of the 17th International Federation of Automatic Control*, pp. 2538–2543, 2008.

[60] A. A. Mamun, T. H. Lee, and T. S. Low, "Frequency domain identification of transfer function model of a disk drive actuator," *Mechatronics*, vol. 12, no. 4, pp. 563–574, 2002.

[61] B. Hredzak, F. Hong, S. S. Ge, J. Zhang, and Z. He, "Modeling and compensation of pivot nonlinearity in hard disk drives," in *Proceedings of the* 16*th IEEE International Conference on Control Applications*, (Singapore), pp. 108–113, 2007.

[62] P. A. Weaver and R. M. Ehrlich, "The use of multirate notch filters in embedded-servo disk drives," in *Proceedings of the American Control Conference*, (Seattle, Washington), pp. 4156–4160, 1995.

[63] D. Wu, G. Guo, and T. C. Chong, "Comparative analysis on resonance compensation in HDD dual-stage actuation systems," *IEEE Transactions on Industrial Electronics*, vol. 50, no. 6, pp. 1179–1186, 2003.

Author's Publications

The contents of this thesis are based on the following papers that have been published, accepted, or submitted to peer-reviewed journals and conferences.

Journal Papers:

1. Phyo Phyo San, Beibei Ren, Shuzhi Sam Ge and Tong Heng Lee, "Adaptive Neural Network Control of Hard Disk Drives with Hysteresis Friction Nonlinearity", *IEEE Transactions on Control Systems Technology*, Accepted, 2009.

Conference Papers:

1. Beibei Ren, Phyo Phyo San, Shuzhi Sam Ge and Tong Heng Lee, "Robust Adaptive NN Control of Hard Disk Drives with Hysteresis Friction Nonlinearity", *Proceedings of the 17th International Federation of Automatic Control*, Seoul, Korea, July 6-11, pp. 2538-2543, 2008.

2. Beibei Ren, Phyo Phyo San, Shuzhi Sam Ge and Tong Heng Lee, "Adaptive Dynamic Surface Control for a Class of Strict-Feedback Nonlinear Systems

with Unknown Backlash-Like Hysteresis", *Proceedings of 2009 American Control Conference*, Hyatt Regency Riverfront, St. Louis, MO, USA, June 10-12 , pp. 4482-4487, 2009.